

Article

Dynamic Response and Failure Mechanism of Concrete Arch Dams under Extreme Loadings: A Solid Foundation for Real-World Actions to Reduce Dam Collapse Losses during Wartime or Terrorist Attacks

Serges Mendo Meye ^{1,*}, Guowei Li ¹, Zhenzhong Shen ², Jingbin Zhang ¹, Ghislain Franck Emani ¹ and Victor Edem Setordjie ³

¹ College of Civil and Transportation Engineering, Hohai University, 1 Xikang Road, Nanjing 210098, China; lgwnj@163.com (G.L.); zhangjingbin2049@hhu.edu.cn (J.Z.); franckemani@yahoo.ca (G.F.E.)

² State Key Laboratory of Hydrology-Water Resources and Hydraulic Engineering, Hohai University, Nanjing 210098, China; zhzhshen@hhu.edu.cn

³ College of Harbor, Coastal and Offshore Engineering, Hohai University, 1 Xikang Road, Nanjing 210098, China; eddyseth@yahoo.com

* Correspondence: mendomos@hhu.edu.cn



Citation: Mendo Meye, S.; Li, G.; Shen, Z.; Zhang, J.; Emani, G.F.; Edem Setordjie, V. Dynamic Response and Failure Mechanism of Concrete Arch Dams under Extreme Loadings: A Solid Foundation for Real-World Actions to Reduce Dam Collapse Losses during Wartime or Terrorist Attacks. *Water* **2022**, *14*, 1648. <https://doi.org/10.3390/w14101648>

Academic Editor: Paolo Mignosa

Received: 18 April 2022

Accepted: 16 May 2022

Published: 21 May 2022

Publisher's Note: MDPI stays neutral with regard to jurisdictional claims in published maps and institutional affiliations.



Copyright: © 2022 by the authors. Licensee MDPI, Basel, Switzerland. This article is an open access article distributed under the terms and conditions of the Creative Commons Attribution (CC BY) license (<https://creativecommons.org/licenses/by/4.0/>).

Abstract: With massive energy demands, the majority of developing countries are at a critical juncture in their industrial development. Their energy structure, on the other hand, is relatively specific and heavily reliant on fossil fuels, resulting in significant environmental pollution. As a result, the development of clean energy is on the horizon, which is related not only to whether developing countries can build a resource-saving and environmentally friendly society but also to whether they can achieve socially sustainable development. As a significant clean energy source, not only does hydropower play an important role in the development of an energy-efficient and environmentally friendly green economy, but it also has numerous benefits such as shipping, irrigation, flood control, and water supply. So, hydropower development is critical for developing countries to adjust their energy structures, achieve regional development balance, and ensure river defense safety. However, precision guidance technology is maturing around the world. If one side's water-retaining dam is accurately blasted in the event of a full-scale war or local conflict, it may cause significant economic and human losses. Dam safety and protection from strong explosions deserve special attention given the obvious seriousness of the consequences. It is critical to improve the anti-explosion safety of major hydraulic structures by revealing the dynamic response behavior, damage mechanism, and dam characteristics under explosion impact loads, as well as evaluating the dam's condition after extreme loads. In the critical work of disaster prevention and mitigation, this is crucial to our social and economic development. This study is not only a key technical problem and an important strategic task in hydraulic structure construction, but it may also serve as a guideline for governments to take effective measures to reduce the loss of dam break under special circumstances.

Keywords: concrete arch dams; dynamic response; damage mechanism; blast loading; failure mode; accumulated damage

1. Introduction

In recent years, the international environment and security situation have deteriorated. At the same time, wars, terrorist attacks, and unintentional explosions occur daily. A review of the world's development pattern reveals that global wars are less likely to occur than local wars. With the advancement of international integration, any country is more likely to be assaulted by international terrorist organizations, posing a serious threat to people's lives and property, as well as a significant menace to the world's economic development

and social stability. As a result, worldwide interest in research on anti-blast and detonation protection of engineering structures has grown.

Currently, research on anti-explosion performance, failure mechanism, and damage characteristics of structures subjected to blast load is primarily focused on civil building structures, ships, and military facilities [1,2]. Several studies on the impact of explosions on structures (dynamic damage constitutive model of concrete, efficient numerical simulation theory and method, anti-explosion safety, and performance evaluation method) were conducted by research teams and relevant research institutions, yielding some results that may be useful in analyzing anti-bang safety problems in dam engineering [3–7]. The structural form, geographical location, protection standards, and requirements of high dam construction, on the other hand, differ from those of civil structures, ships, and military projects.

Arch dams are becoming increasingly popular around the world due to their economic, reasonable, safe, and dependable characteristics. Warfare, terrorist attacks, and unintentional explosions are happening all over the world right now. The study of anti-detonation safety of structures has received a lot of attention in the field of structural protection. The anti-blast fortification of strategic targets such as critical economic, military, and civil infrastructure has posed urgent requirements and challenges to engineering and research institutions. However, as dam engineering technology has advanced, a large number of 100 to 300 m high concrete arch dams have entered the stage of explosive growth. Because of their significant political and economic benefits, high concrete arch dams have undoubtedly become a top focus of local wars or terrorist attacks. If the dam fails, it will cause massive disasters and losses for the nation and its citizens, with inconceivable consequences. The anti-seismic and anti-explosion performance of the dam has become the center of attention during the dam construction and maintenance process. Anti-terrorism has become the top priority of dam safety protection, particularly since the 11 September 2001, terrorist attack. Therefore, taking the bang load as an extreme load and studying the dynamic response, failure mechanism, and anti-burst performance of the high concrete arch dam under the action of blast load can provide a theoretical basis and support for the dam's anti-bang safety evaluation and anti-detonation fortification so that the dam can better play to its economic and military benefits in normal operation, wartime, or terrorist attacks, which have significant military implications.

The dam may be subjected to air explosions from rockets and missiles or underwater explosions from torpedoes, detonators, deep-water bombs, and missiles in terrorist attacks or accidental explosions. However, due to the different physical properties of water and air, as well as the different interface effects with explosion products, the propagation characteristics of an explosion shock wave in water and air differ significantly. As a result, the dam's dynamic response and failure characteristics under underwater and air explosion shock wave loads fluctuate considerably. Therefore, the dynamic response and failure process of the structure under the impact load of underwater and air explosions should be concerned. A dam collapse may cause more damage than a nuclear bomb, and the loss cannot be recovered in a short period.

During World War II, the British Royal Air Force carried out large-scale bombing raids on three dams on the upper Ruhr River in Germany. The explosion blew a large hole in the dams. The induced dam failure caused nearly 400 million tons of floodwater to flow out instantly, resulting in 30,000 deaths or missing people and destroying nearly 200 factories. The entire Ruhr Industrial Zone was razed to the ground, and the nearby arsenal was completely paralyzed, greatly accelerating Germany's defeat and reducing the allies' losses [8]. In 2014, Russian troops demolished a concrete dam in Ukraine's Kherson region to cut off water to Crimea. Before Moscow annexed Crimea, the dam was linked to a canal that supplied 85% of the peninsula's needs [9]. According to Ukraine's infrastructure ministry, on 26 February 2022, at 3:50 a.m., the Ukrainian air defense shot down a Russian missile aimed at the dam of the Kyiv Reservoir. If the dam had been destroyed, the floods could have caused catastrophic casualties and damage, including flooding of residential

areas in Kyiv and the suburbs, according to Ukraine's waterways state enterprise. The collapse of the Kyiv Dam could result in the collapse of the Kaniv, Kremenchuk, and other cascade dams, as well as an accident at the Zaporizhzhya Nuclear Power Plant [10]. A dam strike has incalculable strategic significance in war.

The arch dam's stress characteristic is that the load is transmitted to the rock mass and foundation on both banks through the arch [11,12]. The arch structure's characteristics can save a lot of building materials. Its integrity has also improved. The thickness ratio from the dam bottom to the dam crest is much smaller than that of gravity dams, as is the thickness height ratio. Because of these characteristics, the thickness of the dam body corresponding to the detonation point is not large when the arch dam is subjected to an explosion impact at any point. When compared to the gravity dam, its anti-detonation safety performance will be significantly reduced [13,14]. To summarize, the impact of the burst load on the arch dam's overall shell structure may cause it to collapse in a large area. A high-arch dam has a total storage capacity of nearly 20 billion cubic meters. When the overall regulation fails, a large amount of reservoir water is released instantly, causing unimaginable consequences [11,12]. As a result, research on the safety performance of arch dams under extreme detonation impact loads is an important topic. The structure's response to an explosion load is a complex physical process that includes the explosion of explosive materials, the propagation of a blast shock wave, the dynamic interaction of the shock wave and the structure, and the resulting structural response. The key to determining the mode and magnitude of the bang load in the damage analysis of the dam subjected to the blast impact load is how to determine the mode and magnitude of the detonation load. As a result, a coupling model that fully considers each physical process of an explosion and proposes a calculation method suitable for large scale and high non-linearity is required. At the moment, experimental research and numerical simulation are the major approaches for studying the dynamic response and failure mechanisms of structures subjected to blast impact loads. However, when the test method is used to study the dynamic response and failure mechanism of the dam under an explosion impact load, there are still few test research data and limited test data on the response and failure mechanism of the dam under an explosion load due to limitations in test conditions and test funds, as well as insurmountable disadvantages such as difficult data acquisition, data error, and environmental impact. With the gradual improvement of computer hardware and calculation methods, it is now possible to use a numerical simulation method to simulate the response of an explosion load to a structure.

When using a numerical method to simulate the energy propagation of a blast shock wave, the calculation results are greatly affected by the finite element mesh size. This is because if the mesh is too large, it will have a filtering effect on the shock wave generated by the explosion, resulting in a significant loss of shock energy. Therefore, a smaller mesh size is typically used in the research process. Some researchers believe that, while a mesh size of 500 mm cannot accurately capture the peak pressure generated by the detonation shock wave, the impulse value can [15]. According to research, a mesh size of 200 mm can effectively simulate the impact energy of explosion shock waves. When the detonation distance is long, the mesh size can be increased to meet the requirements of maintaining calculation accuracy while also improving calculation efficiency.

An arch dam is a massive water-retaining structure. The world's highest arch dam currently stands at ≤ 300 m. The dynamic interaction process of the entire arch dam body, reservoir water, air, and foundation system under a bang load is relatively complex and difficult to realize. If a fine mesh size of 200 mm is used for division, the final mesh number will be enormous, and the calculation model will take up a large amount of computer memory. The calculation time will be extremely long, and the calculation result will be enormous, both of which are difficult for ordinary computers to achieve. The dam model is scaled by dimensional analysis. That is, the explosion similarity law is used to simulate the dynamic response and failure characteristics of the arch dam after detonation. It is a feasible scheme to apply the scaling model results to the actual arch dam structure.

Experimenting under the influence of a blast is costly, dangerous, and difficult to collect data from. As a result, numerical methods are used to simulate structural damage and failure caused by an explosion. If a simulation of equal size is used for research on the dynamic response and failure mode of tall buildings under discharge load, the number of meshes will be enormous and the calculation will be impossible to perform. Therefore, the detonation similarity law is required, the dimensional analysis method is used to establish the proportional relationship between various parameters in the blast process, and the numerical simulation analysis of buildings is carried out using the scale model. The law of explosion similarity clearly describes the regular relationship between bang energy and structure damage results, and large structural damage results can be obtained from failure parameters of small structures, and large structure explosion parameters can be converted from the blast phenomenon of small charges.

Because of the serious consequences, the dam's safety and protection from strong explosion impacts are important considerations. Consequently, a fully coupled model of a concrete arch dam under an explosion impact is established in this research paper using Lagrangian and Eulerian coupling methods. Taking into account complex issues such as the high strain rate effect of concrete under the action of an explosion, the dynamic interaction between shock wave and structure, and the dynamic response of the structure, the reliability of the coupling model is validated by comparing it to previous research results. The effects of underwater and air blast shock waves on dam dynamic response, damage degree, damage mechanism, and anti-explosion performance are investigated. The effect of explosive initiation distance, explosive amount, initiation depth, and reservoir water level on the dam's anti-explosion performance is discussed. Simultaneously, based on the damage and failure level proposed in this paper, the most influential factors on the dam's failure state are identified; the typical damage and failure modes and characteristics are obtained for various failure states; the dam damage prediction model under an underwater explosion impact is established, and the dam damage prediction key curve is divided into different failure levels; the dam's safe initiation distance under the impact load of an underwater explosion is determined, and a damage prediction flow chart is provided, which can serve as a foundation and reference for damage prediction of other dam types. Furthermore, the protective effect of foamed aluminum material on the dam body's anti-explosion performance is being studied, which has the potential to significantly reduce the dynamic response and damage of concrete arch dams while also improving their anti-explosion capability. Overall, the results of this study have important theoretical and engineering implications for improving the anti-explosion safety of concrete arch dam structures.

2. Materials and Methods

2.1. The Law of Explosion Similarity

2.1.1. The Law of Similarity of Airborne Explosion

Due to the rapid attenuation of the peak value of the air explosion shock wave, the atmospheric pressure cannot be ignored. Therefore, in air explosions, the peak overpressure is generally used to represent the shock wave pressure at each point. The ideal time history curve of the positive pressure phase of the air blast wave can be expressed as [16]

$$p(t) = P_0 + P_m \left[1 - \left(\frac{t}{td} \right) e^{-\frac{\alpha t}{td}} \right] \quad (1)$$

In the formula, P_0 stands for the atmospheric pressure; P_m denotes the peak value of shock wave overpressure; td represents the duration of the positive pressure stage; α is the

waveform parameter depending on the peak overpressure P_m . For a chemical explosion, Kinney’s peak overpressure can be expressed as:

$$\frac{P_m}{P_o} = \frac{808 \left[1 + \left(\frac{R'}{4.5} \right)^2 \right]}{\sqrt{1 + \left(\frac{R'}{0.048} \right)^2} \sqrt{1 + \left(\frac{R'}{0.32} \right)^2} \sqrt{1 + \left(\frac{R'}{1.35} \right)^2}} \tag{2}$$

where

$$R' = \frac{R}{W^{\frac{1}{3}}} \tag{3}$$

In the formula, R' is the proportional explosion distance; R is the initiation distance, m; W is the quantity of explosive, kg.

The shock wave arrival time t_a is

$$t_a = \frac{1}{C_a} \int_{r_e}^r \left[\frac{1}{1 + \frac{6P_m}{7P_o}} \right]^{\frac{1}{2}} dr \tag{4}$$

In the formula, C_a is the speed of sound in the air medium; r_e represents the radius of the explosive; r stands for the distance from the center of the explosive.

When the shock wave is under positive pressure, t_d is

$$t_d = \frac{980 \left[1 + \left(\frac{R'}{0.54} \right)^{10} \right] \times W^{\frac{1}{3}}}{\left[1 + \left(\frac{R'}{0.02} \right)^3 \right] \left[1 + \left(\frac{R'}{0.74} \right)^6 \right] \left[\sqrt{1 + \left(\frac{R'}{6.9} \right)^2} \right]} \tag{5}$$

The shock wave impulse I (kN·s/m²) [16] is

$$I = \frac{0.067 \sqrt{1 + \left(\frac{R'}{0.23} \right)^4}}{R'^2 \sqrt[3]{1 + \left(\frac{R'}{1.55} \right)^3}} \tag{6}$$

It can also be calculated by the following formula [17]

$$I = \begin{cases} 203R'^{-0.91} & 1 \leq R' \leq 10 \\ 335R'^{-1.06} & 10 \leq R' \leq 200 \end{cases} \tag{7}$$

Meanwhile, other researchers obtained an empirical formula for the peak overpressure of air explosion shock waves based on a large number of tests. Henrych’s empirical formula [18] can be expressed as follow

$$P_m = \begin{cases} \frac{1.40717}{R'} + \frac{0.55397}{R'^2} - \frac{0.03572}{R'^3} + \frac{0.000625}{R'^4} & 0.1 \leq R' \leq 0.3 \\ \frac{0.61938}{R'} - \frac{0.03262}{R'^2} + \frac{0.21324}{R'^3} & 0.3 \leq R' \leq 1 \\ \frac{0.0662}{R'} + \frac{0.405}{R'^2} + \frac{0.3288}{R'^3} & 1 \leq R' \leq 10 \end{cases} \tag{8}$$

Brode’s empirical formula [19] is

$$P_m = \begin{cases} \frac{0.0975}{R'} + \frac{0.1455}{R'^2} + \frac{0.585}{R'^3} & 0.01 < P_m < 1(MPa) \\ \frac{0.67}{R'^3} + 0.1 & P_m > 1(MPa) \end{cases} \tag{9}$$

As a result, when the particle blows up in the air, the particle velocity, impulse, pressure, and other physical quantities on the wavefront satisfy the similarity law with time

and distance. That is, similar blast shock waves will be generated at the same similarity distance as the explosion in the air.

2.1.2. Similarity Law of Explosion in Water

Experiment results have confirmed the existence of an explosion similarity law between the explosion in the air and the explosion impact in the water.

Assuming that the TNT explosive explodes in infinite water, the parameters influencing the propagation of the explosion shock wave in water include the charge radius r , the initial pressure of water P_{w0} , the initial density of water ρ_{w0} , the sound velocity in water c_{w0} , the propagation time of shock wave t , and distance from detonation center R . Therefore, the pressure on the wave surface of a water explosion shock wave can be expressed [20–23].

$$P = f(r, P_{w0}, \rho_{w0}, c_{w0}, t, R) \quad (10)$$

The wave surface pressure can be expressed further as the following functional expression using the π law of dimensional analysis:

$$P = \rho_{w0} c_{w0}^2 \cdot f\left(\frac{P_{w0}}{\rho_{w0} c_{w0}^2}, \frac{t c_{w0}}{r}, \frac{R}{r}\right) \quad (11)$$

If the initial state of the water remains constant during the explosion process, the wave surface pressure function equation can be simplified as follows:

$$P = \rho_{w0} c_{w0}^2 \cdot f\left(\frac{t c_{w0}}{r}, \frac{R}{r}\right) \quad (12)$$

In the above formula, when a certain amount of TNT is exploded in the water, the pressure P at a specific point in the water is only related to the time t when the shock wave reaches this point and the distance R between this point and the detonation center.

If the increase in explosive amount leads to an increase in charge radius by γ times, the time for the shock wave to reach this point at a point γR away from the detonation center will also be magnified by γ times, and the wave surface pressure in this process changes in the same way.

Through a series of underwater explosion experiments, China has amassed a large amount of experimental data in the course of engineering practice [24–27]. On this basis, the empirical formula of the peak pressure P_m of the underwater explosion shock wave is summarized, as follows:

$$P_m = K \left(\frac{W^{\frac{1}{3}}}{R} \right)^\alpha \quad (13)$$

In the formula, K stands for the coefficient of a specific experiment, W is the explosive equivalent, R represents the distance from the detonation center, and α is the attenuation coefficient of peak pressure.

When the US Navy's Surface Weapons Center examined numerous underwater explosion experiments, they developed the empirical formula for underwater explosion parameter ψ , which can be written down as:

$$\psi = K \left(\frac{W^{\frac{1}{3}}}{R} \right)^\alpha \quad (14)$$

In the formula, K represents the coefficient of a specific experiment, W stands for the explosive equivalent, R represents the distance from the detonation center and α is the pressure attenuation coefficient.

The main parameters of underwater detonations are peak pressure P_m , similarity energy flow density $\frac{E}{W^{\frac{1}{3}}}$, similarity impulse $\frac{I}{W^{\frac{1}{3}}}$, and similarity time constant $\frac{\theta}{W^{\frac{1}{3}}}$. Where E

represents the energy flow density, I is the integral of wave surface pressure with time and θ denotes the time constant of exponential attenuation of wave surface pressure.

The following is assumed to be the expression of a pressure wave in water:

$$P(t) = P_m \exp\left(\frac{-t}{\theta}\right) \quad (15)$$

the impulse I can be expressed as:

$$I = \int_0^t P(t) dt \quad (16)$$

The energy flux density E can be expressed as follows:

$$E = \frac{1}{\rho_w c_w} \int_0^t P^2(t) dt \quad (17)$$

The constants and coefficients of the similarity law of explosion in water are also given for TNT explosives. The corresponding K and α of peak pressure P_m are 52.4 and 1.13, respectively; the corresponding K and α of the proportional energy flow density $\frac{E}{W^{\frac{1}{3}}}$ are 84.4 and 2.04, respectively; the corresponding K and α of the proportional impulse $\frac{I}{W^{\frac{1}{3}}}$ are 5.75 and 0.89, respectively; the corresponding K and α of the proportional time constant $\frac{\theta}{W^{\frac{1}{3}}}$ are 0.084 and -0.23 , respectively.

2.2. Underwater and Air Explosion Fully Coupled Model for Arch Dams

To compare and analyze the structural failure effects under underwater and air explosion impact loads, a typical non-overflow section of a concrete arch dam is selected. It is a double-curvature arch dam hydropower project with a total installed capacity of 3.6 million kW, a normal reservoir height of 1880 m, a dead water level elevation of 1800 m, and total reservoir storage of 7.76 billion m^3 . The power station is comprised of permanent buildings for water retention, discharge, and diversion for power generation. Part of the structure is the dam proper, a 305 m concrete double-curvature arch with a maximum dam thickness of 16 m, a maximum dam bottom thickness of 53 m, and a cross-river span of 535 m. It has now been identified as the highest completed dam in the world, four meters higher than the Eiffel Tower in Paris [28]. Figure 1a depicts the contour and size of the optimized arch dam model.

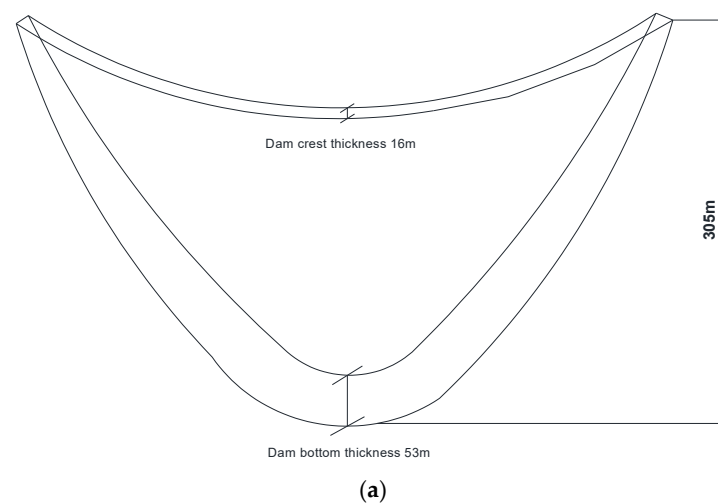


Figure 1. Cont.

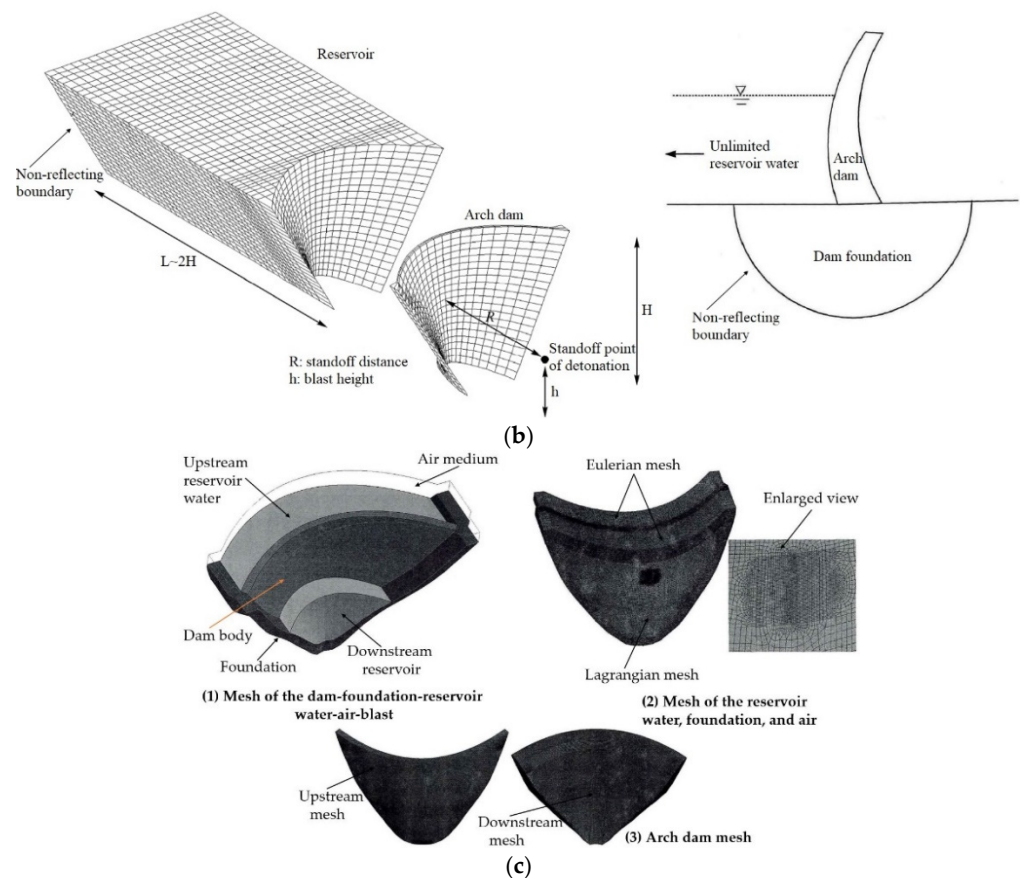


Figure 1. (a) Contour and size of the optimized arch dam model, (b) schematic diagram of the calculation domain, and (c) meshing of the model.

The model includes the coupling of five material models: dam, bedrock, TNT explosive, reservoir water, and air. The unit size of the explosive center and the surrounding medium is set as 100 mm, and the unit size increases appropriately with the increase in the distance from the explosive center. The unit size of the middle and upper part of the dam is 200 mm, and the unit size increases appropriately toward the bottom of the dam. A variety of operating conditions are currently calculated, but this section will present a typical calculation result to analyze the propagation characteristics of shock waves underwater and in the dam structure and the damaging effect of the dam structure under the impact of an underwater explosion.

The developed FORTRAN finite element code is used for all numerical simulations. To involve the important functions, a fully coupled numerical model with combined Lagrangian and Eulerian methods is used, in which the explosive charge, air, and water are modeled using an Eulerian mesh and the solid concrete and rock are modeled using a Lagrangian mesh. The dam body model is reduced by 100 fold using the similarity law of explosions in water and air, and the fully coupled scaled model of the arch dam body-foundation-reservoir water-air-explosive is established using the fluid-structure coupling method, as shown in Figure 1(c₁). Meshes near the dam are divided into 20 mm, while meshes further away are divided into 40 mm. The dam body and foundation are meshed using the Lagrangian method, with a mesh size of approximately 20 mm. Figure 1(c₂,c₃) depicts the specific mesh division. The dam body consists of more than 360,000 mesh units, the reservoir water is made up of more than 330,000 mesh units, the air is composed of more than 190,000 mesh units, the foundation is thought up of more than 20,000 mesh units, and the overall mesh is entirely comprised of 917,926 mesh units. There are approximately 2.75 million degrees of freedom in total.

An iterative partitioned implicit scheme is used in the developed code to time integrate dynamic non-linear equilibrium equations of fluid and structure domains, and an element-by-element preconditioned conjugate gradient solver with diagonal preconditioning is used to solve the large equation system resulting from finite element discretization of the governing equations of fluid and structure domains. When calculating the reservoir water and dam or dam foundation boundaries, the fluid–solid coupling is considered. Figure 1b depicts the domains and boundary conditions of the finite element model. The outer surface of the fluid and dam foundation domain is set to be a non-reflecting boundary in Figure 1b. The dam foundation's bottom is constrained. The element erosion technique is used to simulate the concrete fracture at a principal tensile strain of 0.002 [29,30].

Different mesh divisions are performed for different detonation positions, and fine mesh division is performed for the vicinity of the detonation point so that energy propagation near the detonation point is more accurate. The grid division of the detonation at 40 m underwater near the arch crown beam is depicted in Figure 1(c₂). When the detonation site is 1/4 of the arch ring, the dense grid area is selected at the corresponding part of the detonation center to accurately simulate the explosion shock wave propagation process and reduce workload. Because the arch crown cantilever is located in the middle of the dam body and is a representative part of the dam body's dynamic response, monitoring points are selected at the arch crown cantilever section, 3/4, 1/2, and 1/4 dam heights, which are recorded as monitoring points A, B, C, and D, respectively. Furthermore, 1/8, 1/4, and 3/8 arch rings on the dam's left and right sides are chosen as monitoring points and recorded as monitoring points Z1, Z2, Z3, and Y1, Y2, Y3, respectively, to record the dam's dynamic response to the blast load; the locations of the monitoring points are shown in Figure 2. The failure of an arch dam with different explosive equivalents, including TNT equivalents of 200, 500, 1000, 2000, and 5000 kg, is calculated in this paper to compare calculation results. The damage to an arch dam caused by an explosion in various propagation media, including explosions in water and air, is calculated.

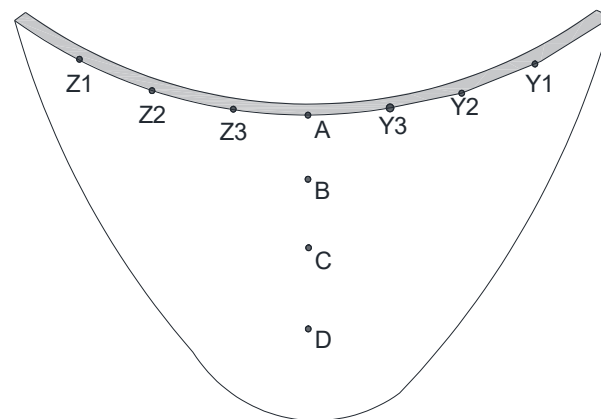


Figure 2. Distribution of monitoring points on the body of the arch dam.

2.2.1. Structural Equations

The second-order equations of motion for solid can be written as

$$\nabla \cdot \sigma + f_s^{ext} = \rho_s \frac{\partial^2 u}{\partial t^2} \quad (18)$$

In the formula, u stands for the displacement of the structure; σ denotes the structural stress tensor; ρ_s refers to solid density; f_s^{ext} is the load vector due to the external structural loads. The equation of motion for solids (Equation (18)) is written in its most general form, which can account for both material and geometric non-linearities. The equation of motion

for the structure subjected to external blast forces can be written in standard finite element form using standard procedures for finite element discretization of the structural domain as

$$M\ddot{u} + C\dot{u} + \int B^T \sigma d\Omega = F_a + F_s \quad (19)$$

In the formula, M and C are the structural mass matrix and damping matrix, respectively; B is a displacement-strain related matrix; σ is the tensor of internal stresses of structure; u is the vector of nodal displacements relative to the ground; F_a and F_s are the vectors of forces associated with the air blast loading and hydrodynamic pressure produced by fluid domain, respectively. Because Rayleigh damping is assumed in this work, the global damping matrix is computed using the expression

$$C = \alpha M + \beta K \quad (20)$$

In the formula, K is the initial stiffness matrix of the dam structure; α and β are reasonableness constants preferred to control the damping ratios of the lowest and highest modes, which are predicted to add significantly to the response. The relationship can be used to calculate these

$$\alpha + \beta\omega_i^2 = 2\omega_i\zeta_i \quad (21)$$

In the formula, ζ_i is the damping ratio and ω_i is the i th natural frequency of the system. The Rayleigh damping method's main disadvantage is that higher modes are significantly more damped than lower modes, and damping can only be controlled for two modes of vibration. In some practical structural problems, mass damping can be ignored and structural damping calculated instead

$$C = \frac{\zeta}{\pi\omega} K \quad (22)$$

In the formula, ω is the main frequency of the structure and ζ is a damping ratio. This current study considers $\zeta = 0.1$.

2.2.2. Fluid Equations

The Euler equations are the set of governing equations that describe the fluid domain in Cartesian coordinates, with viscosity, thermal conductivity, surface tension, and turbulence generally ignored. The total energy equation does not need to be solved directly because the liquid and cavitating fluid are assumed to be compressible and barotropic. These equations are written as follows

The continuity equation

$$\frac{\partial \rho}{\partial t} + \rho_0 \nabla \cdot v = q \quad (23)$$

The momentum equation

$$\rho_0 = \left(\frac{\partial v}{\partial t} + v \cdot \nabla v \right) = -\nabla P + \rho_0 b \quad (24)$$

In Equations (23) and (24), ρ and ρ_0 are the fluid density and the reference density of the fluid, respectively; P is the pressure; v is the fluid velocity vector with three components; b is the body force; and q is the added fluid mass per unit volume and time. With the non-linear convection term $v \cdot \nabla v$, when the fluid velocity is small in comparison to the dimensions of the model, the fluid velocity in the Euler equation can be ignored for the acoustic fluid. As a result, the linearized Euler equation has the form

$$\frac{\partial v}{\partial t} = -\frac{\nabla P}{\rho_0} + b \quad (25)$$

2.2.3. Fluid Domain Application Using Finite Elements

The weak formulation can be written as follows

$$\int_{\Omega_f} \frac{1}{c^2 P} \ddot{P} w d\Omega + \int_{\Omega_f} \nabla P \cdot \nabla w d\Omega = \int_{\Gamma_f} \frac{\partial P}{\partial n} w d\Gamma + \int \rho_f \nabla b w d\Omega - \int \dot{q} w d\Omega \quad (26)$$

In the formula, Ω_f and Γ_f denote the fluid domain and its boundaries. Plugging fluid domain boundary conditions into Equation (26) and representing the unknown with a finite element summing up, $P = \sum_{i=1}^m P_i N_{fi} = P^T N_f$ and assuming $w_i = N_i$ lead to the following set of non-linear ordinary differential equations in time

$$F_f^{int(\ddot{P}, \dot{P}, P)}_f^{ext}(\ddot{u}, b, \dot{q}) \quad (27)$$

For an individual fluid element (e), these are given by the following expressions

$$F_f^{int(\ddot{P}, \dot{P}, P)}_e \left(\int_{\Omega} \frac{1}{2} N_f^T N_f d\Omega + \frac{1}{8} \int_{\Gamma_6} N_f^T N_f d\Gamma \right)_e + \left(\int_{\Gamma_1} \frac{1}{c\beta_1} N_f^T N_f d\Gamma + \int_{\Gamma_2} \frac{1}{c\beta_2} N_f^T N_f d\Gamma + \int_{\Gamma_3} \frac{1}{c\beta_3} N_f^T N_f d\Gamma + \int_{\Gamma_4} \frac{1}{c} N_f^T N_f d\Gamma + \right) \dot{P}_e + \left(\int_{\Omega} \nabla N_f^T \nabla N_f d\Omega + \int_{\Gamma_4} \frac{\pi}{2h} N_f^T N_f d\Gamma \right) P_e \quad (28)$$

and

$$F_{ext}^{int(\ddot{u}, b, \dot{q})}_e \int N_f n N_s^T d\Gamma \ddot{u}_e + F_b(b, \dot{q})_e \quad (29)$$

In the formula, F_{ext}^{int} is the internal force of fluid element, which depends on P and its first two derivatives; F_f^{ext} is the external force; $\Gamma_1, \Gamma_2, \dots, \Gamma_6$ are reservoir boundary surfaces; N_s and N_f are shape functions of structure and fluid domain, respectively; n is normal to the interface and its direction; \ddot{u} is the nodal acceleration produced by the flexible structure; $F_b(b, \dot{q})_e$ is the body force that acts on eth fluid element; β_1, β_2 , and β_3 are acoustic impedance coefficients of material at the bottom, right bank and left bank of the reservoir, respectively. The matrix form of Equation (27) can be written as follow

$$G(p) \cdot \ddot{P} + D(P) \cdot \dot{P} + H \cdot P = -\rho Q^T \ddot{u} + F_f \quad (30)$$

In the formula, $G_{ij} = \sum G_{ij}^e, D_{ij} = \sum D_{ij}^e, H_{ij} = \sum H_{ij}^e$ are matrices representing the mass, damping, and stiffness matrix of the fluid domain, respectively. $F_f = \sum \{F_b\}_i^e$ is the external body force of the fluid domain and $Q_{ij} = \sum Q_{ij}^e$ is the total coupling matrix. \ddot{u}_{total} is the total acceleration along with the interface. The coefficient $G_{ij}^e, D_{ij}^e, H_{ij}^e$, and F_i^e for eth fluid element may be defined as

$$G_{ij}^e(p) = \int_{\Omega} \frac{1}{c(P)^2} \{N_i\}_f^T \{N_j\}_f d\Omega + \frac{1}{8} \int_{\Gamma_6} \{N_i\}_f^T \{N_j\}_f d\Gamma \quad (31)$$

$$D_{ij}^e(P) = \left[\int_{\Gamma_1} \frac{1}{c(P)\beta_1} \{N_i\}_f^T \{N_j\}_f d\Gamma + \int_{\Gamma_2} \frac{1}{c(P)\beta_2} \{N_i\}_f^T \{N_j\}_f d\Gamma + \int_{\Gamma_3} \frac{1}{c(P)\beta_3} \{N_i\}_f^T \{N_j\}_f d\Gamma + \int_{\Gamma_4} \frac{1}{c(P)} \{N_i\}_f^T \{N_j\}_f d\Gamma \right] \quad (32)$$

$$H_{ij}^e = \int_{\Omega} \nabla \{N_i\}_f^T \nabla \{N_j\}_f d\Omega + \frac{\pi}{2h} \{N_i\}_f^T \{N_j\}_f d\Gamma \quad (33)$$

and finally, the coupling matrix is defined as

$$Q_{ij}^e = \int N_s n N_f^T d\Gamma \quad (34)$$

In the integration on the wet interface, the normal vector n is defined to be positive going from solid into the fluid.

2.2.4. System for Non-Linear Fluid–Structure Coupling Coupling between Domains

The forcing terms are used to apply the coupling between the fluid and structural domains. Because the fluid is assumed to be inviscid, the coupling occurs only in the normal direction. The surface traction acting on the fluid as a result of its interaction with the structure is equal to the inverse of the fluid's pressure loading on the structure. The work being done by hydrodynamic pressure on the structure's interaction surface must be equal to the work done by equivalent nodal forces on the fluid element's interface boundary. The coupling matrix (Equation (35)) depicts the relationship between reservoir pressure and dam–reservoir interface forces.

$$QP = F \quad (35)$$

In the formula, F is the force vector acting on the structure due to the pressure loading.

Governing Equations

The finite element discretized equations for the dam–reservoir interaction problem are shown by Equations (19) and (30), which can be written together as

$$\begin{aligned} & \begin{bmatrix} M & 0 \\ -\rho_f Q & G(p) \end{bmatrix} \begin{Bmatrix} \ddot{u}^{n+1} \\ \ddot{p}^{n+1} \end{Bmatrix} + \begin{bmatrix} C & 0 \\ 0 & D(P) \end{bmatrix} \begin{Bmatrix} \dot{u}^{n+1} \\ \dot{p}^{n+1} \end{Bmatrix} \\ & + \begin{bmatrix} K_t & Q \\ 0 & H \end{bmatrix} \begin{Bmatrix} u^{n+1} \\ P^{n+1} \end{Bmatrix} = \begin{Bmatrix} Q(P_i^{n+1} + P_r^{n+1}) \\ F_f \end{Bmatrix} \end{aligned} \quad (36)$$

In the formula, u , \dot{u} and \ddot{u} are the structure nodal displacement vector and its first- and second-time derivatives, respectively; \dot{P} , \ddot{P} , \dot{P} are the hydrodynamic pressure vector of the reservoir domain and its first- and second-time derivatives, respectively. P_i is the impinging shock pressure wave and P_r is the maximum reflected overpressure; K_t , the tangent stiffness matrix of the structural domain, is computed by considering the material non-linearity behavior of concrete and the strain rate effect.

2.3. Non-Linear Dynamic Damage Constitutive Model under a High Strain Rate

2.3.1. HJC Concrete Dynamic Damage Constitutive Model

The concrete material has obvious rate correlation characteristics under the high loading rate of an explosion, and the strain rate is as high as 10/s~103/s [31,32]. Concrete's strength improves significantly when subjected to high strain rates. Holmquist et al. (1993) addressed the dynamic response behavior of concrete under specific conditions such as a high strain rate, large strain, and high confining pressure at the 14th International Ballistic Conference. The Holmquist Johnson–Cook (HJC) concrete dynamic damage constitutive model, based on the Johnson–Cook model, is proposed, which takes into account the strain rate effect, damage degree, and damage softening on the material constitutive relationship. It is adequate to describe the large deformation, the high strain rate, damage, breakage, and fracture of concrete under blast impact loads, as well as equivalent strength models, damage models, and state equations.

The pressure dependence, strain rate effect, and compression damage accumulation of compressive strength are all well taken into account by the HJC constitutive model. The HJC constitutive model, on the other hand, ignores the effects of strain hardening, softening, and the third invariant of stress deviation in concrete materials. As a result, while the HJC constitutive model is appropriate for describing the damage law of materials under compression (for example, good results can be obtained when calculating various concrete penetrations), it lacks an effective description of tensile loading damage.

2.3.2. RHT Concrete Dynamic Damage Constitutive Model

The dynamic response behavior of concrete under blast impact load is extremely complex, with obvious rate-dependent characteristics. Riedel et al. [33,34] proposed the

Riedel–Hiermaier–Thoma (RHT) constitutive model, which was based on the HJC constitutive model. The model describes the variation laws of initial yield strength, failure strength, and residual strength of concrete by introducing three limit surfaces, namely elastic limit surface, failure surface, and residual failure surface. While considering the large strain, the high strain rate, and high-pressure effects of concrete, it also considers the effects of strain hardening, softening, and the third invariant of stress deviation, which can describe the entire process of concrete from elasticity to failure; it is widely used to simulate the dynamic response characteristics as well as damage and fracture problems of brittle materials such as concrete and rock under high strain rate dynamic loading.

2.3.3. JH-2 Rock Foundation Dynamic Damage Constitutive Model

Johnson and Holmquist proposed a constitutive model to simulate the dynamic response behavior of brittle materials under large deformation, a high strain rate, along with high temperature and pressure (Johnson–Holmquist, JH model [35]). This model was improved from the Johnson–Cook model [36]. Since the JH model does not account for the progressive softening of materials, Johnson and Holmquist improved the JH model and proposed the JH-2 model [37]. When studying the dynamic interaction between dam and bedrock, the JH-2 model, which is mainly composed of a state equation, strength model, and damage model, is used to consider the dynamic characteristics of bedrock.

2.3.4. Coupling Model Validation

Due to a lack of test data, the failure test of a reinforced concrete slab under blast impact performed by other researchers [38] is used as a reference in this paper to verify the accuracy and reliability of the numerical model used to analyze the dynamic response and damage failure of the concrete arch dam under blast impact load. The numerical model of a reinforced concrete slab subjected to blast impact load is developed in strict accordance with the test conditions. The numerical calculation results will be compared with the model test results [38] to ensure that the numerical model used in this paper is correct.

2.3.5. Dynamic Damage Model of Arch Dam Blast Loads

With the gradual advancement of computer hardware and calculation methods, numerical simulation methods can now be used to simulate the response of explosion loads to structures. In this paper, the numerical simulation method is used to reproduce the existing test failure process, which is then used to validate the numerical model's reliability. A three-dimensional numerical model should be used to analyze the overall and local failures of reinforced concrete slabs to more realistically simulate and predict the failure mode of reinforced concrete slabs under blast impact loads. A fully coupled model of a reinforced concrete slab under explosive impact is established using Lagrangian and Eulerian coupling methods based on the experimental parameters of reference [38]. Because of the model's symmetry, only 1/4 of the model is established for analysis. The Eulerian mesh, which has high accuracy, is used to simulate TNT explosives and air. To improve calculation efficiency, the Lagrangian mesh simulates the concrete slab and reinforcement; to consider the dynamic interaction between air and a reinforced concrete slab, the fluid–structure coupling algorithm is used; concrete, reinforcement, explosive, and air all have a unit size of 5 mm. The shock wave is transmitted at the truncated boundary of the air domain, and no energy is reflected in the calculation region, thanks to the application of an outflow boundary around the air. Because the action time of an explosion impact load is so short, the bond between reinforcement and concrete is usually assumed to be intact. When establishing the reinforced concrete slab model, the common joint between reinforcement and concrete is considered, and the separation condition of the section is the failure of concrete or reinforcement element. For concrete materials, the RHT constitutive model is used, and for reinforcement, the Johnson–Cook material model [36] is used. This model is appropriate for describing the mechanical behavior of materials under conditions of large deformation, a high strain rate, and high temperature.

2.4. Anti-Explosion Protection Measures for Arch Dams

In the event of war, the high concrete arch dam is easily attacked by the enemy, and if the dam is destroyed by a devastating blow, the country and its people will face serious disaster. As a result, it is necessary to investigate arch dam anti-explosion measures to improve the protection performance of arch dams against blast attacks. In general, an arch dam's anti-blast performance can be improved in two ways: (1) the application of a protective layer to the surface of a concrete structure; (2) the use of high-performance explosion-proof damming materials. There has been little research on the anti-bang measures of a high concrete arch dam up to this point. The method of foaming aluminum on the dam's upstream surface is used in this paper to study the anti-blast performance of high concrete arch dams and to provide a valuable reference for the high concrete arch dam's detonation-proof safety design.

Aluminum foam (the porous metal based on aluminum and its alloys) has been known for more than a half-century, but its distribution and application are still limited. The main reason for this was the low reproducibility of structure and material properties in aluminum foam production. Some of these challenges have been overcome thanks to the advancement of aluminum foam technology. Several processes for producing metal foams have been developed and studied [39]. This porous structure determines the physical properties of aluminum foam, which have low density, high porosity, and a large surface area ratio, making aluminum foam widely used in energy dissipation, shock absorption, anti-knock, and anti-impact applications.

In the study of anti-explosion measures of concrete gravity dam, foam concrete is added upstream of the dam as a measure to improve the anti-explosion performance of the dam. Compared with aluminum foam, foamed concrete has the advantage of low price, but the protection efficiency of foamed concrete is not high. For a gravity dam, adding foamed concrete in front of the dam can play a certain protection effect and has little influence on the overall shape of the dam body. For an arch dam, if foamed concrete is used as anti-explosion material and foamed concrete with 2 m thickness is added in front of the dam, the original dam type will be greatly changed, which will bring much inconvenience to design and construction. Foamed aluminum outperforms foamed concrete in terms of anti-knock performance [40–42]. The elastic modulus of the commonly used foamed aluminum material is 1.2 GPa, the Poisson's ratio is 0.3, and the tensile strength is 10 MPa, whereas the foamed concrete material has an elastic modulus of 342.2 MPa, the Poisson's ratio is 0.1, and the tensile strength is 0.20 MPa. The anti-knock performance of the two is vastly different. The crushable foam constitution or honeycomb structure model is commonly used in numerical studies to simulate aluminum foam [43,44]. A compressible foam model with isotropic hardening properties is represented by the crushable foam constitutive equation. The model is capable of describing the mechanical behavior of aluminum foam when compressed [45]. If the elastic modulus of aluminum foam is constant and the modified stress has elastic properties, then [46]:

$$\sigma_{ij}^t = \sigma_{ij}^n + E \varepsilon_{ij}^{n+\frac{1}{2}} \Delta t^{n+\frac{1}{2}} \quad (37)$$

When the test principal stress value $\sigma_i^t (i = 1, 3)$ exceeds the compacted stress σ_c , that is, $|\sigma_{ij}^t| > \sigma_c$, then:

$$\sigma_i^{n+} = \frac{\sigma_c \cdot \sigma_i^t}{|\sigma_i^t|} \quad (38)$$

In the formula, E is the elastic modulus, σ_i^t is the test stress, and $\sigma_i^t (i = 1, 3)$ is the test principal stress.

The engineering stress–strain curve of the input material is required for the constitutive relationship of aluminum foam, as shown in Figure 3. The stress–strain curve of aluminum foam can be divided into three stages, as shown in the figure: elastic deformation, plastic yielding, and compaction.

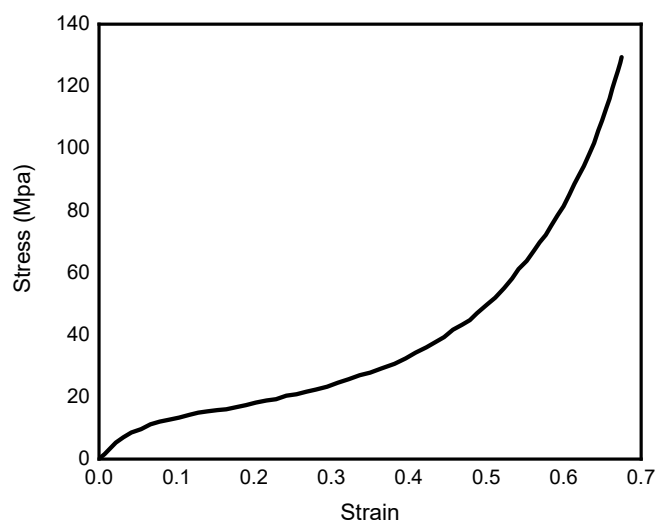


Figure 3. Foam aluminum constitutive curve.

Under the action of the explosive load, the foamed aluminum begins to compress. Through the compaction deformation of the cell pore structure, the deformation energy of the blast wave is transformed into the strain energy of the aluminum foam, reducing the energy of the blast shock wave on the structure and achieving the function of protecting the structure.

3. Results and Discussions

3.1. Comparison and Analysis of Numerical and Experimental Results

Using the Lagrangian and Eulerian coupling methods, the damage diagram of a reinforced concrete slab subjected to a blast impact load is obtained. In Figure 4, a numerical simulation of the damage and failure of a reinforced concrete slab under the initiation impact of 0.31 kg TNT is shown and compared to experimental results in the literature [38]. Some radial and circumferential cracks appear on the blast-facing surface of concrete slabs as a result of blast impact load, as shown in Figure 4a, which is similar to the test results shown in Figure 4b. The shock wave will reflect and form a tensile wave as it spreads to the bottom of the reinforced concrete slab. Because of the low tensile strength of concrete, the reinforced concrete slab's back bursting surface will collapse and crack, as shown in Figure 4c. The test results in Figure 4d also show that seismic collapse failure occurs at the bottom due to tensile waves, and the numerical simulation results show the same development trend and range of cracks.

The comparison of numerical calculation results and test results of reinforced concrete slab failure under a 0.46 kg explosive initiation impact load is shown in Figure 5. As shown in Figure 5, as the amount of explosive increases, so does the cracking and failure range of a reinforced concrete slab's blasting face and back blasting face. The cracking distribution diagram obtained by numerical simulation of the blasting face and back blasting face of concrete slabs is consistent with the distribution law of the test results.

The results of the above analysis show that the crack distribution of reinforced concrete slabs obtained by the numerical simulation method is consistent with the distribution law of test results and that the process of cracking, crack propagation, and bottom seismic collapse of reinforced concrete slabs under the action of an explosion impact load can be well showcased. It demonstrates that the numerical model used in this paper can accurately predict the dynamic response and failure process of structures subjected to a blast impact load.

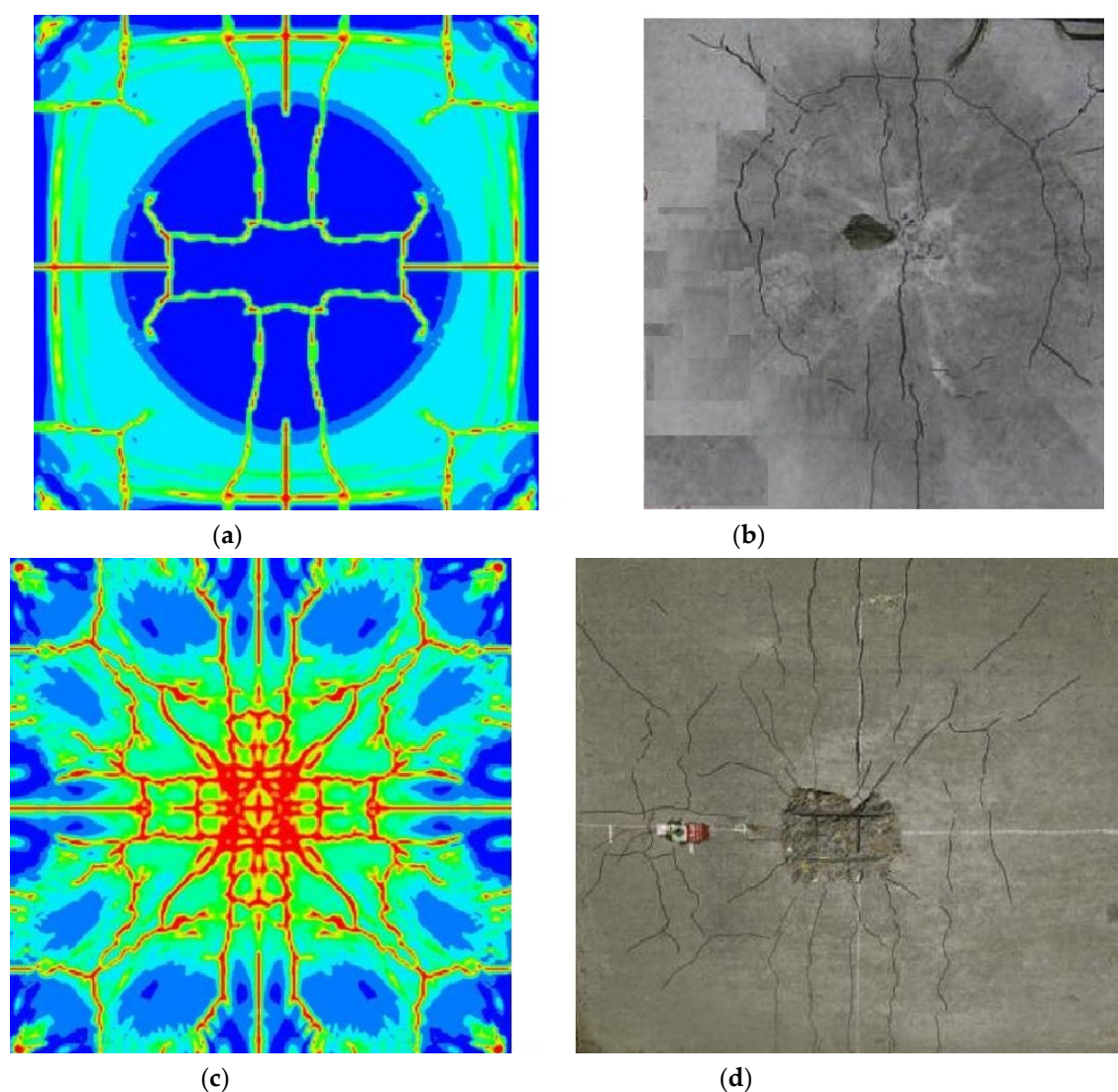


Figure 4. Failure of strengthened concrete slabs under a 0.31 kg TNT blast impact. (a) Numerical calculation results of blasting face; (b) test results of blasting face. (c) Numerical results of the back blasting face; (d) test results of the back blasting face.

3.2. Underwater and Air Explosion Impact Damage Characteristics of a Concrete Arch Dam

Underwater and Air Explosion Shock Wave Propagation

Because of the large differences in physical properties such as density, sound velocity, and compressibility between water and air, as well as the different interfaces between explosion products and water and air media, there are substantial variations in the propagation characteristics of an explosion shock wave in water and air. When numerical methods are used to investigate the explosion shock wave propagation process, the numerical calculation results are highly dependent on the finite element mesh size. In general, smaller numerical meshes yield more accurate results. However, due to the limitations of existing computer hardware and software, the calculation becomes difficult when the mesh size is small enough for the mass concrete arch dam. The precision of the numerical calculation results is low when the mesh size is too large. Luccioni et al. [47] analyzed the performance of mesh size on the simulation and prediction of explosion loads using fluid mechanics software and concluded that a mesh size of 100 mm could accurately simulate the propagation law of explosion loads, whereas a larger mesh size could only quantitatively simulate the propagation law of explosion loads in a complex urban environment. Zhou and Hao [48] predicted the peak pressure and impulse of the protected structure using mesh sizes of 500

and 250 mm, respectively, and believed that while the larger mesh size could not accurately capture the peak pressure of the explosion shock wave, it could approximate the impulse of the explosion shock wave.

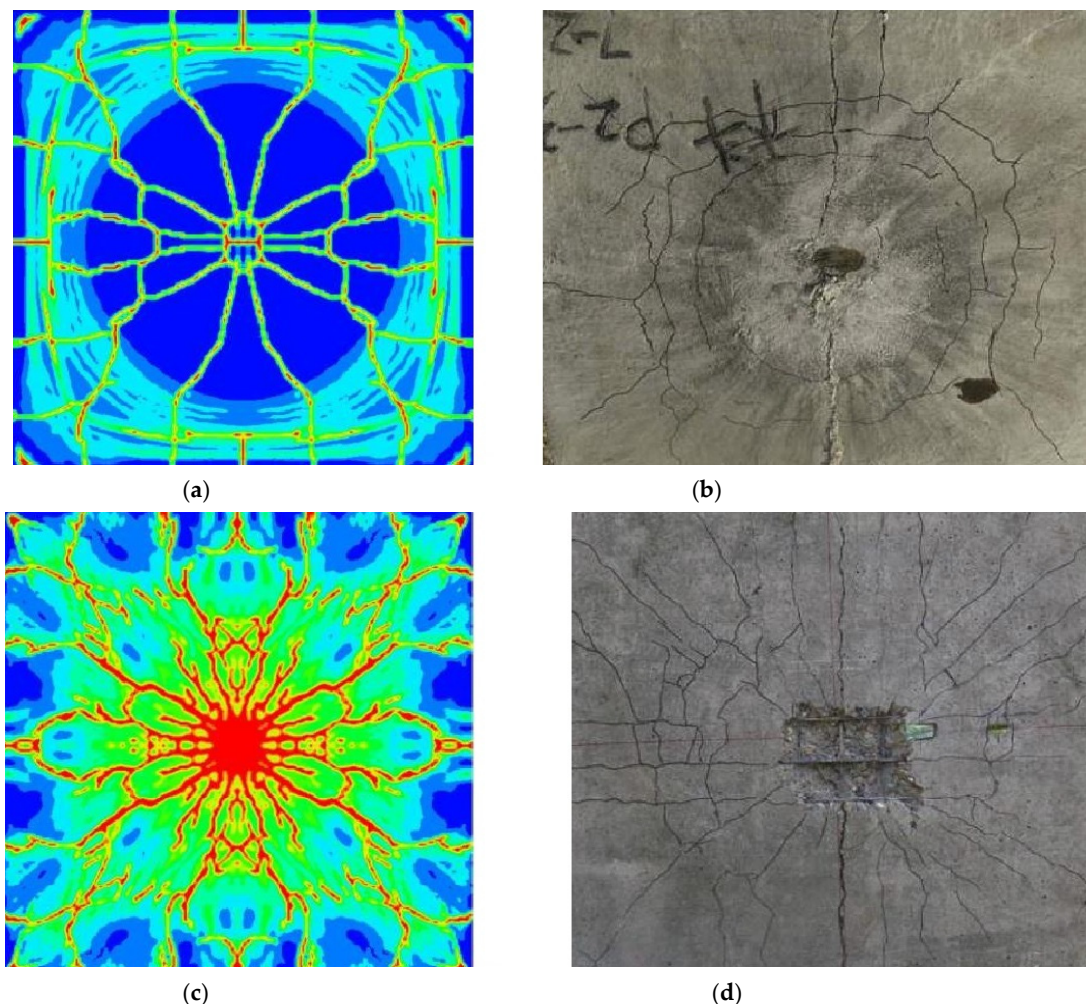


Figure 5. Failure of strengthened concrete slabs under a 0.46 kg TNT blast impact. (a) Numerical calculation results of blasting face; (b) test results of blasting face. (c) Numerical results of the back blasting face; (d) test results of the back blasting face.

This section will establish three-dimensional free field underwater and air explosion finite element numerical calculation models with different mesh sizes, compare and analyze the propagation process and characteristics of underwater and air explosion shock waves, as well as the influence of different mesh sizes on the calculation, to verify the reliability of the numerical model and compare the propagation characteristics of underwater and air explosion shock waves. 1/8 of the model is used for calculation and analysis to save calculation time and storage space. The 3D model's symmetry axes are X, Y, and Z, and the calculation area is $10\text{ m} \times 10\text{ m} \times 10\text{ m}$. The total number of computing meshes is 1,125,000, respectively. TNT explosive material weighs 1000 kg, and the detonating point is in the center of the explosive. For water, air, and explosives, the Eulerian algorithm is used. The Eulerian algorithm can be used to describe the behavior of liquids and gases. Because the interface between the free edge interface and the material is represented by a fixed Eulerian mesh, large deformation or flow will not result in mesh distortion. The model is artificially truncated at a certain distance from the explosive center to reduce the calculation workload. An outflow boundary is applied at the artificial truncation boundary

to simulate the free field explosion so that the shock wave is transmitted at the artificial truncation boundary with no energy reflected in the calculation area.

When the mesh size is 100 mm, Figure 6 depicts a typical pressure–time history curve at a specific point of an underwater and air explosion (the explosion center distance is 5 m). As shown in the figure, there is a difference in the propagation characteristics of the shock wave in the two media when the explosive is detonated underwater and in the air. After the shock wave shows up, the pressure rapidly goes up to a peak (the overpressure peak is 2.16 MPa) and then decays quasi-exponentially to the surrounding atmospheric pressure, which is known as the positive pressure phase. When the shock wave attenuates to atmospheric pressure, it does not stop, but rather continues to attenuate, and a negative pressure stage occurs. The shock wave pressure in the negative pressure stage is frequently small in comparison to the peak value of shock wave overpressure in the positive pressure stage. When using the simplified air explosion shock wave load for structural dynamic response analysis, the effect of pressure in the negative pressure area is generally overlooked, and only the effect of positive pressure overpressure is accounted for. When a shock wave arrives in a water explosion, the pressure instantly rises to a peak and decays exponentially, similar to the positive pressure stage of an air explosion, and the positive pressure action time is shorter than that of an air explosion. The shock wave’s peak pressure is 85.58 MPa or approximately 39.62 fold that of an air explosion.

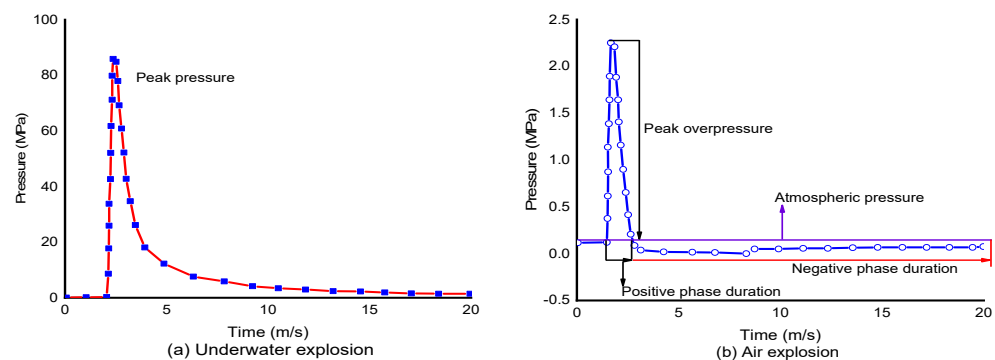


Figure 6. Typical pressure–time history curve at 5 m from the detonation’s center.

Figure 7 depicts the shock wave peak pressure (overpressure peak) and shock wave impulse curves of underwater and air explosions. The figure shows that the peak pressure and impulse obtained by an underwater explosion are much greater than those obtained by an air explosion, and the peak attenuation of overpressure obtained by an air explosion is much faster than that obtained by an underwater explosion, owing to the direct dissipation of air explosion energy into the surrounding atmosphere. The figure also shows that the shock wave attenuation process is large with increasing explosion center distance, the peak value of the shock wave pressure near the explosive is large, and the attenuation is fast with increasing explosion center distance. The average pressure peak and impulse of an underwater explosion shock wave are 42.35- and 71.99-fold higher, respectively, than those of an air explosion.

Mesh sizes of 100 and 200 mm were used for the 3D free-field underwater model and the air explosion model, respectively, to assess the mesh size effect of the 3D model. To validate the numerical model’s reliability, the numerical calculation results are compared to the empirical formulas of Cole [49] and Ford K & Graham [50]. Figure 8 depicts the relationship curve and empirical values between the peak pressure of an underwater and air explosion shock wave and the explosion center distance with different mesh sizes.

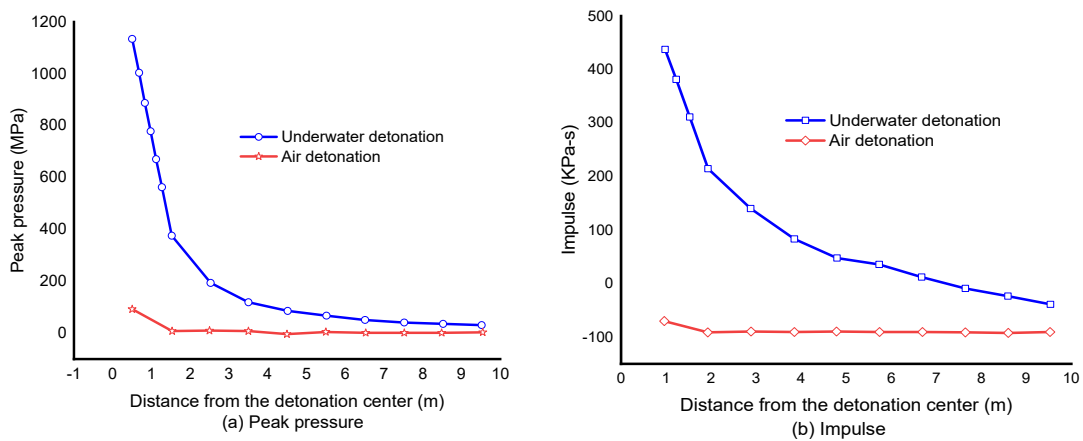


Figure 7. Comparison of peak pressure and impulse of underwater and air explosion shock waves.

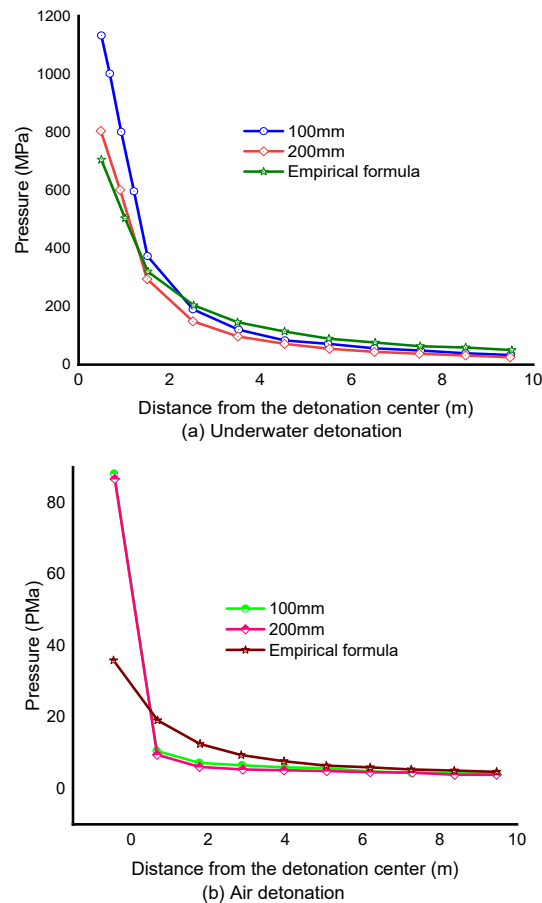


Figure 8. The effect of mesh size on shock wave peak pressure.

When comparing the numerical calculation results with the empirical values, it is easy to see that there is a certain gap between the numerical calculation results under different mesh sizes and the empirical values, as shown in the figure. Except for the monitoring points near the explosive center, the empirical values of shock wave pressure of underwater and air explosions are larger than the numerical results, due to the big size of the numerical model mesh, but they are generally close to the empirical values, and the gap narrows as one moves away from the explosion center. Although reducing the mesh size of the numerical model can improve the calculation accuracy of shock wave peak pressure, it will require a lot of calculation workload and higher and higher computer configuration requirements. The numerical model's peak pressure of the shock wave near the explosive

center is much higher than the empirical value, owing to the proximity of the explosion center. The shock wave's peak pressure is very high, the measurement error of the test is high, and the numerical model is also difficult to accurately capture the shock wave pressure near the explosive center, which is affected by the mesh size.

Figure 9 depicts the relationship between the shock wave impulse of underwater and air explosions and the detonation center distance for various mesh sizes and provides empirical values. Except for the points near the explosive center of the air explosion, the shock wave impulse obtained by the numerical model under different mesh sizes is close to the empirical value, indicating that, while the numerical model does not accurately capture the shock wave peak pressure generated by underwater and air explosions (which is close to the empirical value overall), it can effectively simulate the shock wave impulse. When the distance from the blast center is great, the calculation efficiency can be greatly improved by appropriately increasing the mesh size of the numerical model, and calculation accuracy can be guaranteed.

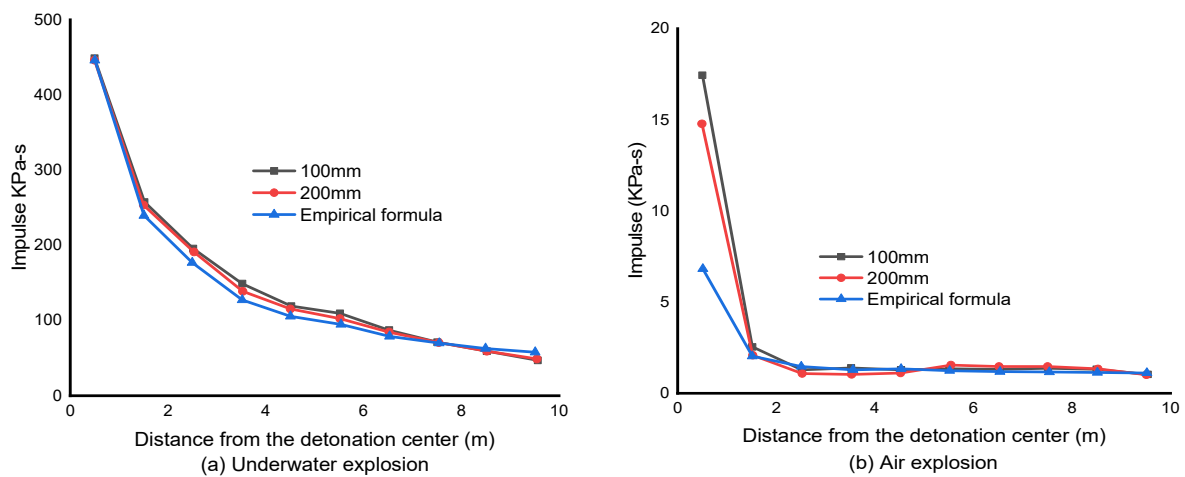


Figure 9. Mesh size effect of a shock wave impulse.

3.3. An Underwater Explosion Impact Load on the Anti-Explosive Performance of a Concrete Arch Dam

The underwater explosion shock wave has a high peak pressure and a short duration, and the destructive effect of an explosion shock wave propagating in water is much stronger than that of an explosion shock wave propagating in air, which is why dam structures are easily damaged. As a result, the underwater explosion shock load influences the dam's dynamic response and destructive effect. To discuss the anti-detonation performance of a concrete arch dam under the action of an underwater explosion impact load, a fully coupled model is designed to study the influence of explosive initiation distance, explosive quantity, and initiation depth on the anti-detonation performance of the concrete arch dam. Furthermore, the possible failure mode, corresponding failure mechanism, and failure characteristics of the concrete arch dam under an underwater explosion impact load are discussed, and the influence of reservoir front water level on the failure mode and anti-explosion performance of the dam is analyzed, which can be used as a reference for engineering application and damage assessment.

3.3.1. The Effect of Explosive Quantity on the Anti-Knock Performance of a Concrete Arch Dam

The shock wave load acting on the structure is directly proportional to the charge of high-energy explosives, and the number of explosives used in accidental explosions and potential terrorist attacks varies. To study the impact of different bomb charges on the anti-explosion performance of the arch dam, it is assumed that the detonation depth is uniformly set to 10 m underwater, the detonation distance is 10 m, and the detonation

point is located on the section of the arch crown cantilever, as shown in Figure 10. The dam height is 305 m and the reservoir water level height is 285 m. The bomb charges are 200, 500, 1000, 2000, and 5000 kg, respectively. The failure mode of a concrete arch dam under an underwater explosion impact load is obtained.

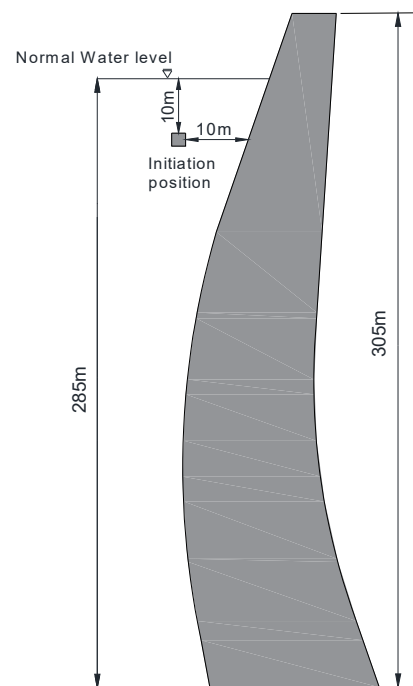


Figure 10. Position of detonation at various explosive equivalents.

When the initiation depth and center distance of the bomb remain constant, the amplitude of the impact load on the dam surface subjected to an underwater explosion increases with the amount of explosive used. The damaged area and depth of the dam body's upstream surface gradually increase as well, and dam damage is usually serious. When the amount of explosives is increased further, the dam body suffers severe damage. The damaged area of the dam body is increasing in size, and the dam body's water-retaining capacity is deteriorating as a result of the explosion.

The dam failure modes at various levels of explosion are as follows:

1. When 200 kg of TNT is detonated, the upstream surface of the dam body near the center of the explosion is slightly damaged. The damaged area is not very large, and the depth of the damage is approximately 0.6 m. On the downstream surface, there is a tensile damage area near the elevation of the detonation center. This is because the impedance of the concrete at the downstream surface to the wave is much greater than that of the air when the shock wave propagates from the upstream surface to the downstream surface inside the dam. As a result, the bang shock wave will reflect on the downstream surface, forming a strong reverse tensile wave. This local tensile stress exceeds the concrete's tensile strength, and a certain range of tensile failure will form at the downstream surface. The distribution of tensile damage is broad, but the damaged depth is small (approximately 2.4 m). At the same time, the downstream surface has a larger damaged area than the upstream surface because the tensile damage caused by the explosion shock wave propagating in the dam body has a wider distribution than the compressive damage. The foundation surface has minor damage. In general, the explosive load produced by 200 kg of TNT does not affect the dam body's stability, and the dam body can continue to operate normally after repair.
2. When 500 kg of TNT is detonated, a certain amount of damage occurs on the dam body's upstream surface near the detonation center. In addition, there is a small area of

contiguous damage on the dam body's downstream surface. The downstream surface has a larger damaged area than the upstream surface. The accumulated damage from the dam body vibration caused by the blast wave effect accounts for a portion of the damage at the dam crest. The superposition of tensile damage done by shock wave reflection and crushing damage caused by the detonation shock wave results in damage to the downstream surface. The foundation surface has some damage, but given the stress characteristics of the arch dam, the thrust force of reservoir water in front of the dam will be transmitted to the rock mass on both sides through the arch ring, so the dam can still be considered safe to operate.

3. When 1000 kg of TNT is detonated, the dam crest damage has obvious interval distribution characteristics, and the dam crest and foundation surface damage are larger. The damaged area at the dam body's downstream surface is also significantly larger than when TNT is 500 kg. The damage expansion range is wider, and the damage distribution on the dam body is symmetric.
4. When TNT weighs 2000 kg, the explosion causes extensive damage to the existing roof and in the middle of the arch crown cantilever. The downstream surface of the dam body has a large area of continuous damage, and the damaged area of the downstream surface is larger than that of the upstream surface. A section of the dam body near the dam's top has penetrating damage and has lost its water-retaining capacity.
5. When 5000 kg TNT is detonated, the arch crown cantilever section suffers from a wide range of tensile damage. The upper half of the dam body collapses, the dam loses its water-retaining capacity, and the reservoir water instantly empties.

To better describe dam damage, the upstream damage area ratio is the ratio of the area with an upstream damaged value greater than 0.5 to the total area of the upstream surface. The downstream surface's damage area ratio can be calculated in the same way. The dam crest damaged volume ratio is the ratio of the volume of the area with a damaged value of more than 0.5 within 50 m of the dam crest to the total volume of this area. Table 1 shows the impact of explosive equivalent weight on the explosion-proof capacity of the dam body by listing the damage to the dam body, such as the damaged area ratio of upstream and downstream surfaces, the damaged depth of the arch crown cantilever, and the damaged volume ratio of the dam crest under different explosive charges. As shown in Table 1, as the explosive charge increases, so does the damaged area of the upstream and downstream surfaces. The downstream surface of the dam body has a larger damaged area than the upstream surface. In addition, the damaged volume ratio of dam crest positions continues to rise. When the explosive volume is 5000 kg, almost all of the dam crest positions are damaged, the dam body loses its ability to retain water, and the damaged depth of the dam body gradually increases until it completely penetrates the dam body.

Table 1. Failure of the arch dam under various explosive equivalents.

Explosive Equivalent (kg)	Damaged Area Ratio (%)		Damaged Depth of Crown Cantilever (m)		Dam Crest Damaged Volume Ratio (%)
	Upstream Face	Downstream Face	Upstream Face	Downstream Face	
200	1.4	6.5	0.6	2.4	1.8
500	7.9	11.7	2.8	2.6	9.7
1000	12.8	21.2		Penetration	41.1
2000	30.3	38.7		Penetration	79.6
5000	42.5	88.4		Penetration	91.7

Because the dam crest is severely damaged, it must be addressed forcefully. The damage within 10 m below the dam crest is averaged along the arch direction for different explosive charges.

The damaged distribution curve is drawn along the arc length of the dam crest, as shown in Figure 11. The damage at the dam crest, as shown in the figure, exhibits the distribution characteristics of interval areas, particularly when the explosive equivalent

weight is 500 kg and 1000 kg. The dam crest damage curve reflects the main dam crest damage location characteristics and has a symmetrical distribution with the bang point as the center. This feature also reflects the mode-shaped participation characteristics that may exist at the arch dam crest under blasting load.

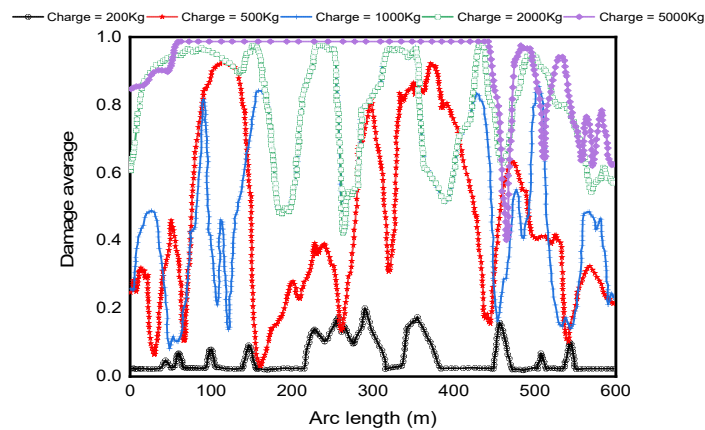
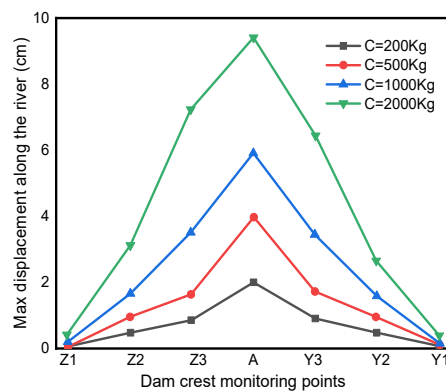
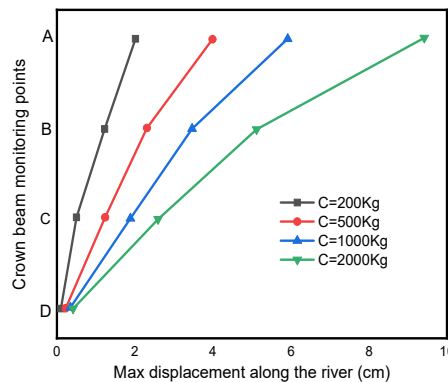


Figure 11. Dam crest damage curve with different explosive charges.

The maximum values of displacement, velocity, and acceleration of each monitoring point at the dam crest and arch crown cantilever in the entire dynamic time history are extracted to further study the dynamic response of the dam body under different explosive equivalents, as shown in Figure 12. When the explosive weight is 5000 kg, almost all of the dam crest positions are damaged, and some of them are blown up, causing their displacement to increase indefinitely. As a result, 5000 kg of TNT is not included in the figure.

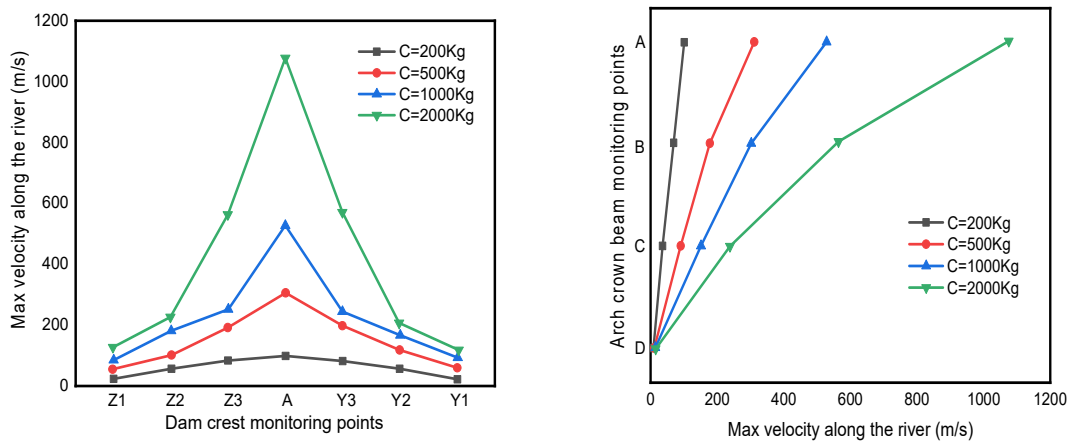


(a) Max displacement of the dam crest monitoring points along the river



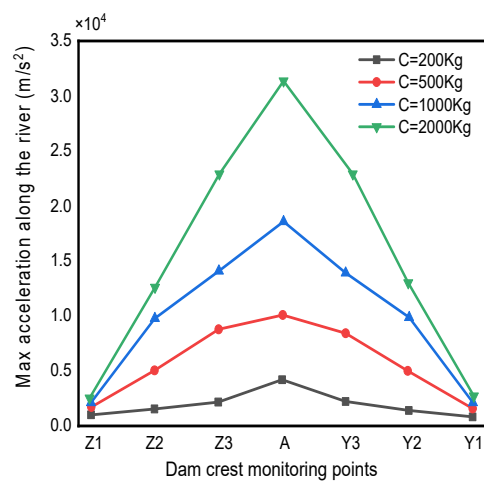
(b) Max displacement of arch crown beam monitoring points along the river

Figure 12. Cont.

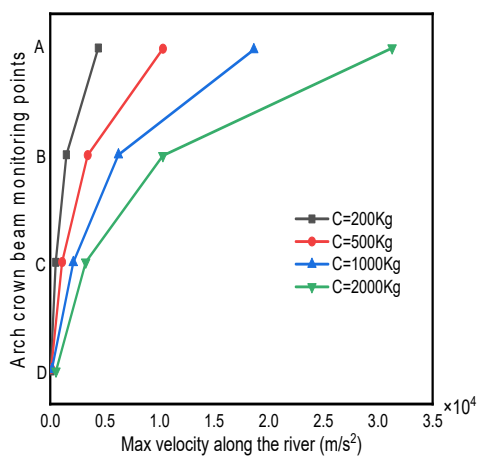


(c) Max velocity of dam crest monitoring points along the river

(d) Max velocity of the arch crown beam monitoring points along the river



(e) Max acceleration of the dam crest monitoring points along the river



(f) Max acceleration of the arch crown beam monitoring points along the river

Figure 12. Dynamic response of monitoring points with different TNT amounts.

As shown in Figure 12, as the explosive equivalent weight increases, so do the maximum values of displacement, velocity, and acceleration at each monitoring point. The initiation center is located at the height of 275 m dams of the arch crown beam. For the monitoring points on the dam top, the dynamic response of the monitoring points at the arch crown beam is the most intense. The closer the monitoring point is to the arch end, the farther it is from the initiation center, and the less the dynamic response is. The dynamic response of the monitoring points on the arch crown cantilever is most intense at the top of

the arch crown cantilever, and the closer to the monitoring point at the bottom of the dam, the farther away from the detonation center, the less dynamic response to the explosion. It is clear that when the shallow water near the arch crown cantilever blasts, the dynamic response at the top of the arch crown cantilever is the most severe, owing to the dam body's weak explosion proofing.

The above analysis shows that, due to the structural characteristics of the arch dam itself, the impact effect of a small amount of explosive on the dam body is not significant, because the dam body transmits a large portion of the pressure to the rock mass on both banks. Due to the small thickness of the dam concrete, the detonation impact will cause a wide range of penetrating damage to the dam body and directly cause a dam collapse when subjected to high explosive content. As long as the damage on the dam's downstream surface is caused by tensile damage reflected by the burst shock wave, its distribution is wider than the damage on the dam's upstream surface. However, the overall damage depth is not great. The dynamic response of the dam body increases as the explosive charge increases, and the top position of the arch crown cantilever is the most sensitive to the explosion impact, which is the dam body's weak point. As a result, precautions should be taken to safeguard the dam's top position.

3.3.2. Influence of Different Detonation Media on the Dynamic Response and Damage Failure of the Arch Dam

The damage to the dam body is affected by the different detonation media. That is, the dam body may sustain varying degrees of damage as a result of the explosion in air and water. When the detonation media is air or water, the dynamic response and damage failure of the dam body are calculated separately. In the case of various detonation media, the discharge center is uniformly set at 275 m or 30 m below the top. In the event of an air blast, the dam body upstream and downstream is completely exposed to the air. That is, no water flows upstream or downstream of the dam body. The detonation point in the water bang is 10 m underwater. The detonation distance is 10 m, the TNT weight is 1000 kg, and the blast position is shown in Figure 13 on the section of the arch crown cantilever.

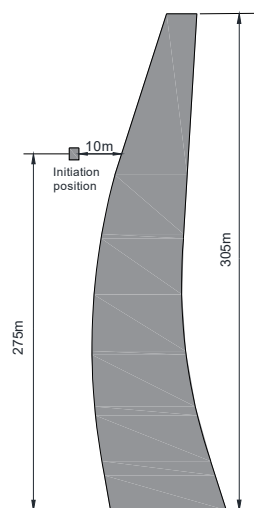


Figure 13. Positions of detonation for various media.

The damage caused by the explosion in the air to the dam body is much smaller than that caused by the blast in the water under the same explosive equivalent and detonation position.

The upstream and downstream surfaces of the dam body, the dam crest, and the dam foundation sustain extensive damage in the event of a water burst. The upstream surface of the dam near the detonation center is slightly damaged when it explodes in the air, and the damaged depth is approximately 2 m. There is also minor damage, with a damaged depth

of approximately 2 m near the arch ends on both sides of the dam's downstream surface. When different detonation media are detonated, the damaged area ratio of upstream and downstream surfaces of the dam, the damaged depth of the arch crown cantilever, and the damaged volume ratio of the top of the dam body are listed, so that the influence of the detonation media on the anti-detonation capacity of the dam can be more clearly seen, as shown in Table 2.

Table 2. Damage of arch dams under various blast media.

Blast Media	Damaged Area Ratio (%)		Damaged Depth of Arch Crown Cantilever (m)		Dam Crest Damage Volume Ratio (%)
	Upstream Face	Downstream Face	Upstream Face	Downstream Face	
Air	2.5	3.6	2.0	-	2.7
Water	12.8	21.2	Penetration		41.1

As shown in Table 2, when the detonation position is the same but the detonation medium is different, the damage caused by blasting in the air is much smaller than that caused by detonation in water, regardless of the damaged area ratio of upstream and downstream surfaces, the damaged depth of the arch crown cantilever, or the damaged volume ratio of the dam crest.

Arbitrating from the dynamic response of each dam body monitoring point, the dynamic response of the dam body exploding in the water, whether it is displacement, velocity, or acceleration along the river, is much larger than that in the air.

To recap, the dynamic response and dam body damage in an air explosion are much lower than in a water explosion. As a result, when the dam is inevitably subjected to blast load impact, the bang should be avoided in water as much as possible to improve the dam's anti-burst performance.

3.4. Research on Influencing Factors of Anti-Explosion

3.4.1. The Effect of Detonation Depth on the Anti-Explosion Performance of a Concrete Arch Dam

Because the concrete arch dam is a mass concrete structure, the superstructure is brittle, while the substructure is thick and stiff. When the reservoir water level remains constant, the projectile will detonate at various initiation depths, and the shock wave generated will act on different parts of the dam, influencing the dynamic response and failure mode of the dam. A concrete arch dam is chosen as the research object to investigate the impact of explosive initiation depth on the anti-explosion performance of the dam. The dam's height is 305 m, and the reservoir's depth is 285 m. The detonation depth of explosives has a clear impact on the dam's body damage. Therefore, the dynamic response and dam body damage are calculated for detonation depths of 0, 40, 80, 140, and 200 m, and the failure mode of a concrete arch dam under an underwater explosion impact load is obtained. This section establishes a fully coupled finite element model for the detonation depths of 10, 40, 80, 140, and 200 m, respectively, to improve the accuracy of the energy propagation simulation near the detonation point when the explosion occurs, and finely divides the mesh near the detonation point, which not only accurately simulates the blast shock wave propagation process but also reduces workload. The detonation distance is uniformly set at 10 m for all detonation depths, TNT weight is 1000 kg, and the blasting position is located on the arch crown cantilever section, as shown in Figure 14.

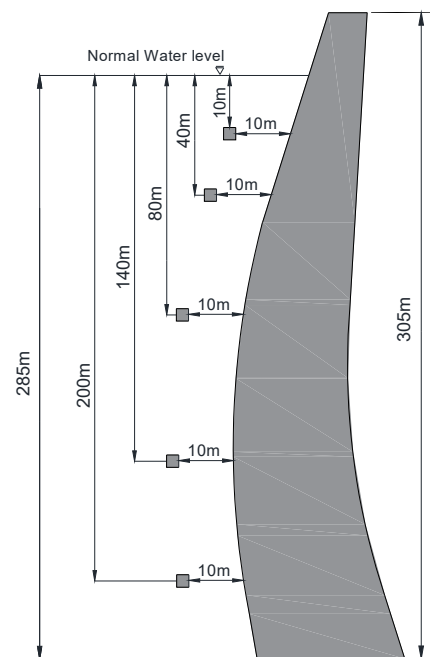


Figure 14. Detonation positions at various detonation depths.

The analysis results show that as detonation depth increases, the main damaged position of the dam body's upstream surface continues to move downward, and the damaged area near the elevation of the detonation center of the upstream surface continues to decrease. The damaged area of the upstream surface is significantly smaller than that of the downstream surface near the detonation center, and the overall damaged volume of the arch dam continues to decrease as the detonation depth increases.

When the detonation depth is 10 m, an obvious damaged area with a radius of approximately 15 m appears on the dam's upstream surface near the detonation center. The upstream dam crest is continuously damaged, with a damaged depth of approximately 8 m and the length of the main damaged area accounts for approximately 70% of the length of the arch crown ring. The damaged area of the dam body's downstream surface is mainly focused at the dam crest near the arch crown cantilever. The damaged area's center is located along the river's axis in the direction of the detonation center. A portion of the pressure damage at the arch dam's foundation surface is caused by compression damage to the dam concrete when the explosion impact load is transmitted to the rock mass on both banks via the crown arch ring.

When the detonation depth is 40 m, there is damage in the corresponding area upstream of the detonation center elevation with a radius of approximately 18 m. However, the degree of damage is significantly lower than when the detonation depth is 10 m. The dam crest on the upstream surface has contiguous damage with an estimated damage depth of 8 m and the length of the main damaged area accounts for approximately half of the length of the top arch ring; the damage on the dam body's downstream surface is primarily concentrated in the dam's center; the depth of the damage is nearly 6 m, and the damaged area is relatively concentrated. The other damage is mostly concentrated at the shoulder position, at both ends of the top arch ring, with the right arch end nearly crushed. Overall, the dam body suffers less damage than when the detonation depth is 10 m.

When the detonation depth is 80 m, the damage to the dam body's upstream surface is concentrated primarily in the vicinity of the detonation center along the river axis. The damaged area has a radius of approximately 18 m, and the damage degree is lower than when the detonation depth is 10 m. There is continuous damage at the dam crest, with a damaged depth of approximately 7 m, and the length of the main damaged area accounts for approximately half of the length of the crown arch ring. The left and right bank arch end downstream of the dam body have been damaged to a depth of approximately 4 m, and

the foundation surface of the left bank at the elevation of the detonation center has been damaged to a depth of approximately 12 m. All in all, the dam body suffers less damage than at detonation depths of 10 and 40 m.

When the detonation depth is 140 m, the elevation of the center of the damaged area on the dam body's upstream surface is reduced further, and the radius of the damaged area is approximately 7 m. The dam top's damaged depth is approximately 8 m, and the length of the main damaged area accounts for approximately 40% of the length of the crown arch ring. The damaged area on the dam body's downstream surface is approximately at the same elevation as the detonation center, and the damaged depth is approximately 3 m. There is damage to the foundation surface of the left bank at the elevation of the detonation center to a depth of approximately 10 m. The overall damage to the dam body is less than that caused by detonation depths of 10, 40, and 80 m.

When the detonation depth is 200 m, the damage to the dam body's upstream surface is significantly reduced. The radius of the damaged area is only approximately 3 m, the damaged depth at the dam crest is approximately 4 m, the damage distribution is relatively scattered, and the main damaged area's length does not exceed 15% of the length of the crown arch ring. The damaged area on the dam body's downstream surface is approximately at the same elevation as the detonation center. The damaged depth is no more than 3 m, and there is damage to the arch ends on both sides with a depth of no more than 5 m. Overall, the dam body is less damaged than at detonation depths of 10, 40, 80, and 140 m.

Table 3 shows the damaged area ratio of upstream and downstream surfaces, the damaged depth of arch crown cantilevers, and the damaged volume ratio of the dam crest at various detonation depths, allowing the impact of the detonation depth on the anti-discharge capacity of the dam body to be more clearly seen.

Table 3. Arch dam body damage at various detonation depths.

Detonation Depth	Damaged Area Ratio (%)		Damaged Depth of Crown Cantilever (m)		Dam Crest Damage Volume Ratio (%)
	Upstream Surface	Downstream Surface	Upstream Surface	Downstream Surface	
10	12.8	21.2	Penetration		41.1
40	10.6	22.7	8.8	5.8	37.3
80	11.5	14.4	4.8	0.2	27.6
140	9.6	10.3	4.6	3.2	19.4
200	4.2	5.8	0.4	2.0	8.7

Table 3 shows that as the detonation depth increases, the damaged area ratio of the dam body's upstream and downstream surfaces continues to decrease, as does the damaged volume ratio of the dam crest position. This demonstrates that as the detonation depth increases, the degree of damage caused by the blast shock wave to the dam body decreases. This is because as the detonation depth increases, so does the thickness of the horizontal position of the dam corresponding to the detonation point, resulting in relatively weakened dam damage. However, the damaged area ratio of the upstream surface is smaller than that of the downstream surface.

Since the dam crest location damage is more severe, it must be the subject of discussion. Under different detonation depths, the damage within 10 m below the dam crest is averaged along the dam crest's arch direction, and the dam crest's damage distribution curve along the arc length is drawn, as shown in Figure 15. The figure shows that the damage at the dam crest displays the distribution characteristics of interval areas. The dam crest damage curve reflects the dam crest's main damage location characteristics, which present a symmetrical distribution with the explosion point as the center.

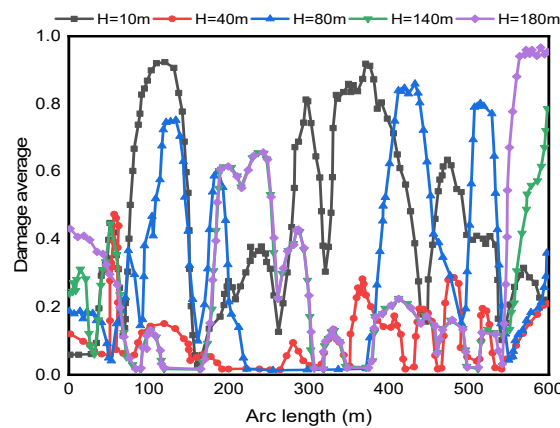


Figure 15. Dam crest damage curves for various blasting depths.

The maximum values of displacement, velocity, and acceleration of each monitoring point at the dam crest and arch crown cantilever in the entire dynamic time history are extracted to further investigate the dynamic response of the dam body under different detonation depths, as shown in Figure 16, where H stands for the detonation depth.

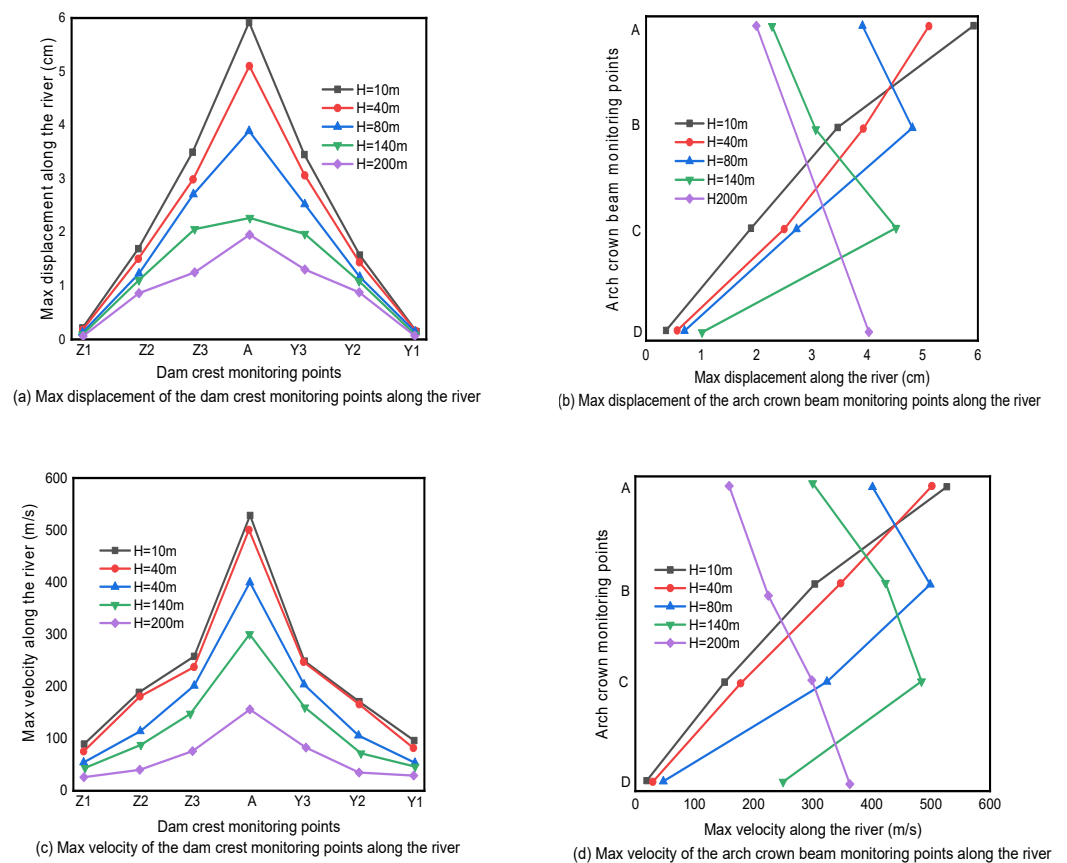


Figure 16. Cont.

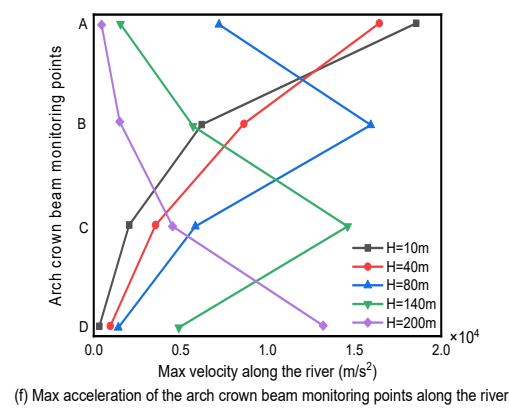
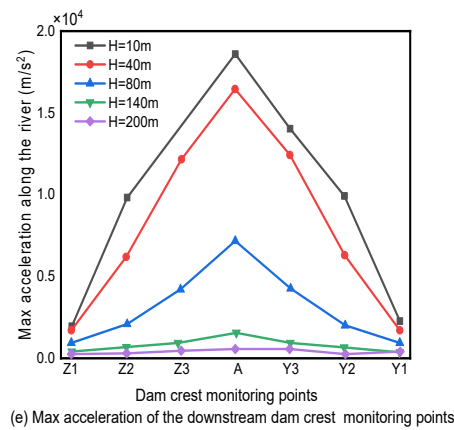


Figure 16. Dynamic response of monitoring points at different detonation depths.

The maximum values of displacement, velocity, and acceleration of dam crest monitoring points along the river are shown in Figure 16 to be larger in the middle and smaller on both sides. Furthermore, the greater the detonation depth, the weaker the dynamic response of each dam crest monitoring point. When the detonation depth reaches 200 m, the maximum values of displacement, velocity, and acceleration at the dam crest are approximately 3-, 4-, and 20 times lower, respectively, than when the detonation depth is 10 m.

The maximum displacement, velocity, and acceleration values at each monitoring point at the arch crown cantilever position shall be taken as the peak near their respective detonation points, with the force increasing the opening of the detonation depth. When the detonation depth is 10 m, the detonation center is near point A, and the maximum values of displacement, velocity, and acceleration are taken at point A. The detonation center is located between points A and B when the detonation depth is 40 m. As a result, the maximum value of displacement, velocity, and acceleration at monitoring point A is slightly lower than that at detonation depth of 10 m, while the maximum value of displacement, velocity, and acceleration at monitoring point B is slightly higher. When the detonation depth is 80 m, the detonation center is near point B, and the maximum value of each monitoring point’s displacement, velocity, and acceleration is taken at point B. When the detonation depth is 140 m, the detonation center is near point C, and the maximum value of each monitoring point’s displacement, velocity, and acceleration is taken at point C. When the detonation depth is 200 m, the detonation center is near point D, and the maximum value of each monitoring point’s displacement, velocity, and acceleration is taken at point D. This proves that the bang impact load has the most obvious influence on the dynamic response of the monitoring point closest to the detonation center, while the influence on the dynamic response of the monitoring point farthest from the detonation center is relatively weak. The greater the distance, the less powerful the influence.

3.4.2. Influence of the Blast Distance on the Blast Protection Behavior of Concrete Arch Dams

Because the shock wave of an underwater explosion decays exponentially with increasing propagation distance, when the initiation distance from the explosive to the target structure varies, the shock wave load acting on the structure varies greatly. As a result, this section will study the effect of various detonation distances on the failure mode and anti-blast performance of concrete arch dams. The research object is an actual concrete arch dam. The dam's height is 305 m, and the reservoir's normal water level is 285 m.

The detonation distance of the blast has a significant impact on the dam body's failure. Therefore, when the variation range of the detonation distance is 1, 10, and 20 m, the dynamic response and damage failure of the dam body are calculated. The detonation depth is uniformly set at 40 m at different discharge distances, TNT weight is 1000 kg, and the ignition position is located on the section of the arch crown cantilever, as shown in Figure 17.

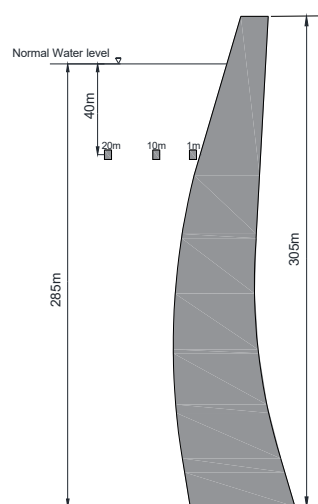


Figure 17. Position of detonation at various detonation distances.

When the TNT explosive quantity and initiation depth are kept stable, analysis reveals that as the detonation distance increases, the peak pressure of the dam subjected to an underwater blast shock wave gradually decreases, the dam's dynamic response weakens, and the damage range decreases: Explosion pit failure, cavitation punching failure, collapse tensile failure, shock wave punching failure, and overall tensile failure are the most common types of dam failure.

When the explosive explodes near the dam's upstream surface (1 m), the high-pressure shock wave generated by the underwater explosion has a short propagation distance. When it acts directly on the dam's upstream surface, the concrete is compressed and yields, and it is crushed first to form an explosion compression funnel pit; punching shear damage occurs on the upstream surface of the dam near the free water surface and extends to the downstream approximately horizontally as a result of the water cut-off effect, resulting in penetrating crack damage; due to the structural stress characteristics of the dam, punching failure occurs in the vicinity of bang crater failure, with approximately two main cracks extending diagonally to the dam inner surface; because the wave impedance of the concrete medium is much greater than that of air when the shock wave propagates to the downstream surface, it will reflect and form a strong tensile wave. However, the tensile strength of concrete is much lower than the compressive strength, and collapse and tensile failure will occur at the dam body's downstream surface. Because the explosive is close to the dam's upstream surface, the shock wave energy is primarily used to destroy the dam superstructure, causing reservoir water to overflow the damaged area and rush downstream instantly.

When the detonation distance is 10 m, the dam near the free water surface is damaged by cavitation punching damage due to the cut-off effect of the free water surface. The damage extends to the interior of the dam body and penetrates with the collapse tensile damage caused by a strong tensile wave on the downstream surface, resulting in penetrating damage and dam cracking. In the corresponding area upstream of the detonation center elevation, there is damage with a radius of approximately 18 m. The upstream dam crest has continuous damage with a damage depth of approximately 8 m, and the length of the main damaged area accounts for approximately 50% of the length of the crown arch ring. The damage on the dam body's downstream surface is largely focused on the dam's center. The depth of the damage is approximately 6 m, and the damaged area is relatively concentrated. Another damage is focused on the dam abutment at both ends of the top arch ring, and nearly all of the right arch ends have been crushed. The damaged area on the upstream side is smaller than the damaged area on the downstream side near the detonation center. To sum up, the dam body sustains less damage than the detonation distance of 1 m.

The damage range is further reduced when the detonation distance is reduced to 20 m. The peak pressure of the underwater explosive shock wave decreases exponentially as the propagation distance increases, and the impact load acting on the dam is small, with small punching damage mainly occurring on the dam's upstream surface. Due to shock wave reflection, tensile damage failure occurs at the downstream surface. There is only damage with a radius of approximately 4 m in the corresponding area of the upstream surface of the elevation of the detonation center, and there is scattered damage at the dam crest. When the detonation distance is 10 m, the depth and range of damage at the arch end on both sides are smaller. The dam body as a whole can maintain stable operation, and no dam break will occur as a result of excessive local damage.

When the damaged area ratio of upstream and downstream surfaces, the damaged depth of the arch crown cantilever, and the damaged volume ratio of the dam crest are measured at different detonation distances, the influence of the detonation distance on the anti-explosion ability of the dam body is more fully evident, as shown in Table 4. The damaged area ratio of the upstream surface is less than that of the downstream surface as a whole, as shown in Table 4. The damaged area ratio of the dam's upstream and downstream surfaces decreases as the detonation distance increases, as does the damaged volume ratio of the dam crest, and the damaged depth of the arch crown cantilever decreases from penetrating to shallow damage. This fully demonstrates how, as the detonation distance increases, the dam damage can be effectively reduced. Under various detonation distance conditions, the damage within 10 m below the dam crest is averaged along the dam crest's arch direction, and the dam crest's damage distribution curve along the arc length is drawn, as shown in Figure 18. The dam crest damage curve reflects the dam crest's main damage location characteristics and has a symmetrical distribution centered on the blast point. At the same time, it can be seen that when the detonation distance is 1 m, the dam's crest is almost destroyed.

Table 4. Arch dam body damage at various blasting distances.

Detonation Distance (m)	Damaged Area Ratio (%)		Damaged Depth of Crown Cantilever (m)		Dam Crest Damage Volume Ratio (%)
	Upstream Surface	Downstream Surface	Upstream Surface	Downstream Surface	
1	19.5	41.2	Penetration		74.6
10	10.6	22.7	8.8	5.8	37.3
20	2.7	5.1	2.6	0.0	4.9

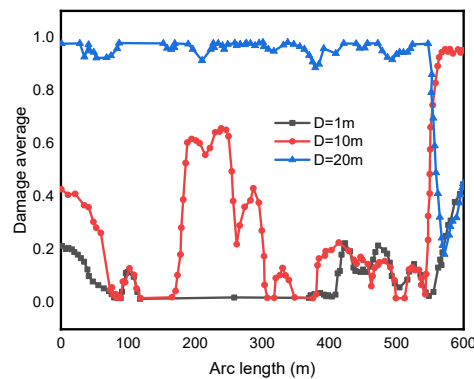


Figure 18. Damage curves of dam crest at different blasting distances.

The closer the detonation distance, the greater the maximum value of displacement, velocity, and acceleration along the river of each monitoring point on the dam crest and arch crown cantilever, and the more intense the dynamic response of the dam body, according to the dynamic response of the dam body monitoring points.

3.4.3. Arch Dams’ Dynamic Response and Failure Mode at Various Horizontal Detonation Positions

The detonating position of the explosive has a clear impact on the dam body’s failure. Therefore, to improve the accuracy of the simulation of energy propagation near the detonation point when the explosion occurs, the dynamic response and failure of the dam body are calculated in this section when the detonating positions at the arch crown cantilever are 3/8, 1/4, and 1/8 of the arch ring, respectively. A fully coupled finite element model is established, and the mesh near the detonation point is finely divided, which not only accurately simulates the blast shock wave propagation process but also reduces workload. As shown in Figure 19, the detonation depth is uniformly set at 40 m, the detonation distance is 10 m, and the TNT weight is 1000 kg for different detonation locations.

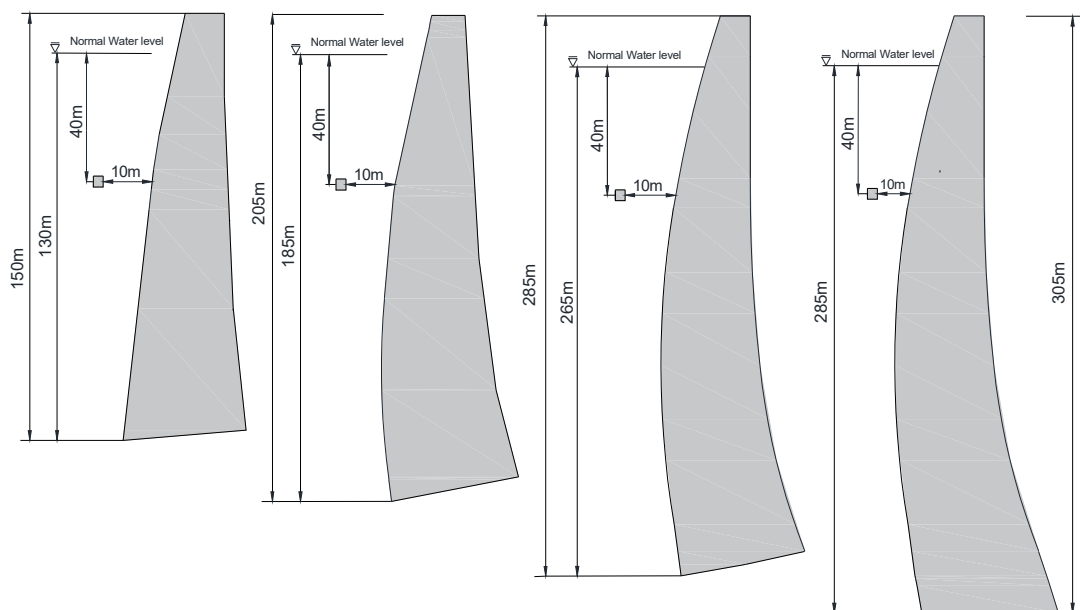


Figure 19. Positions of detonation at various levels.

The dam body’s damage at different horizontal detonation positions is recorded, such as the damaged area ratio of upstream and downstream surfaces, the damaged depth of section at detonation position, and the damaged volume ratio of the dam top, so that the

influence of horizontal detonation position on the dam body's anti-detonation ability can be seen more clearly, as shown in Table 5.

Table 5. Arch dam body damage at various horizontal blast positions.

Horizontal Detonation Position	Damaged Area Ratio (%)		Damaged Depth of Crown Cantilever (m)		Dam Crest Damage Volume Ratio (%)
	Upstream Surface	Downstream Surface	Upstream Surface	Downstream Surface	
Crown cantilever	10.6	22.7	8.8	5.8	37.3
3/8 arch	8.8	16.2	4.8	0.4	22.7
1/4 arch	10.2	14.8	2.0	8.2	20.6
1/8 arch	6.4	15.2	4.4	0.0	16.8

According to Table 5, the horizontal detonation position has a significant effect on the dam body's anti-knock ability. When the detonation position gradually shifts from the section of the arch crown cantilever to one side, the damaged area ratio of the dam's upstream and downstream surfaces as a whole shows a decreasing trend, as does the damaged volume ratio at the dam crest. Moreover, the upstream surface's damaged area ratio is significantly lower than that of the downstream surface. Based on the foregoing, it can be concluded that the detonation near the arch crown cantilever is the most damaging to the dam body's anti-blasting ability.

The damage distribution curve along the arc length of the dam crest position is drawn by taking the average value of the damage within 10 m below the dam crest along the arch direction of the dam crest under the condition of different horizontal detonation positions, as shown in Figure 20. The dam crest damage curve demonstrates that the main damage locations at the dam crest have clear interval distribution characteristics.

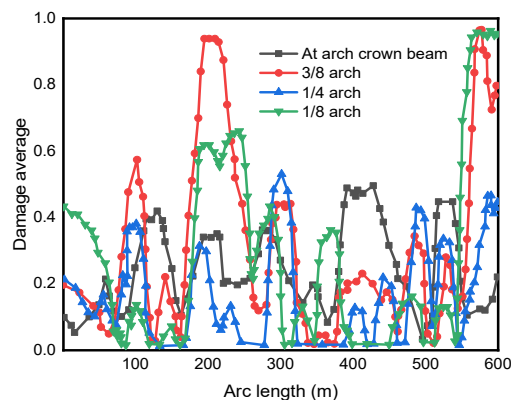


Figure 20. Dam crest damage curve for various horizontal blast positions.

The maximum values of displacement, velocity, and acceleration in the full dynamic time history of each monitoring point at the dam crest are extracted to further investigate the dynamic response of the dam body under different initiation positions, as shown in Figure 21. As shown in Figure 21, as the initiation center moves from the arch crown cantilever to the side arch end, the maximum value of displacement, velocity, and acceleration at the dam top also moves from the arch crown cantilever to the side dam end. When the detonation center is near the arch crown cantilever, i.e., near point A, the maximum value of displacement, velocity, and acceleration of each monitoring point on the dam crest is taken at point A. When the detonation center is at the 3/8 arch position, that is, close to the Z3 point, the maximum value of displacement, velocity, and acceleration of each monitoring point on the dam crest is taken at the Z3 point. When the detonation center is located at the 1/4 arch position, that is, near the Z2 point, the maximum value of displacement, velocity, and acceleration of each monitoring point on the dam crest is taken at the Z2 point.

When the detonation center is located at the 1/8 arch position, that is, near the Z1 point, the maximum value of displacement, velocity, and acceleration of each monitoring point on the dam crest is taken at the Z1 point.

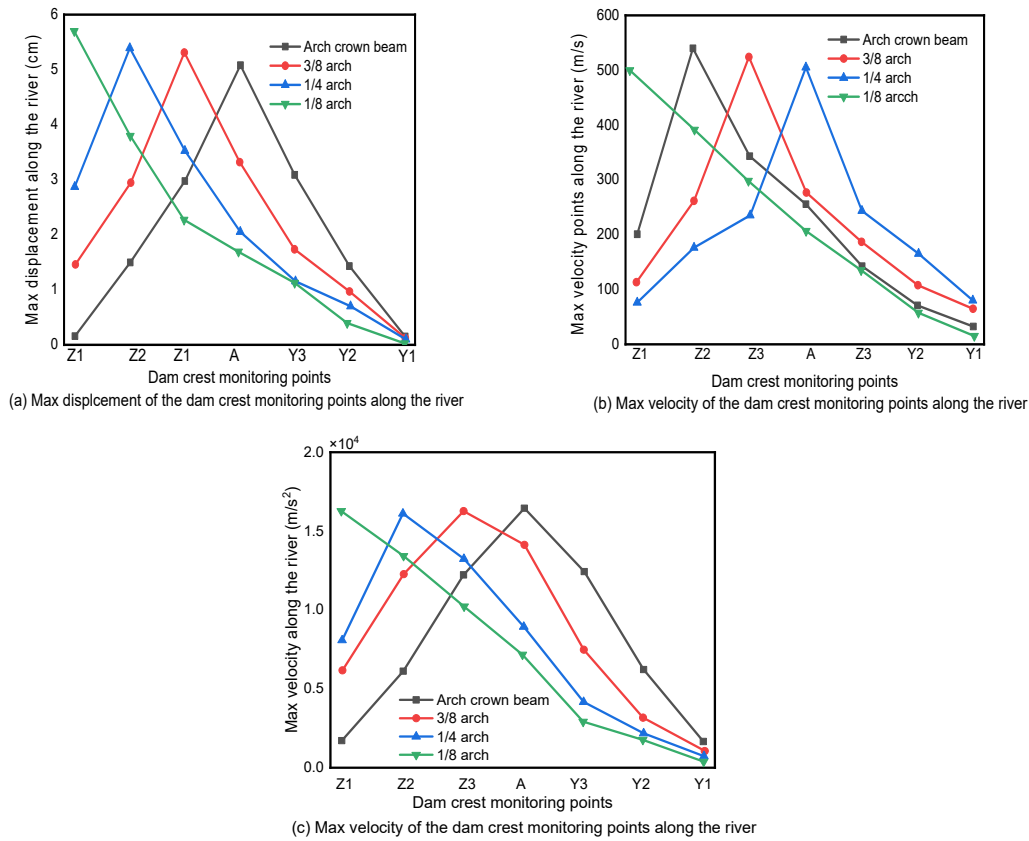


Figure 21. Dam crest monitoring points’ dynamic response at various horizontal detonation positions.

3.4.4. The Effect of the Reservoir’s Water Level on the Anti-Explosion Performance of Concrete Arch Dams

There are indications of modern warfare, and major water conservancy infrastructures, as the first key targets of general warfare, can implement civil air defense measures for early warning and water release. The influence of the reservoir water level in front of the dam on the anti-explosion performance of the dam after early warning water release is studied using the non-overflow section of a concrete arch dam as the research object. Different water levels in front of the dam have a strong influence on the dam body’s failure. So, the dam body’s dynamic response and the damage caused by the explosion are computed. This section establishes the finite element full coupling model when the water level in front of the dam is the normal water level, the water level drops by 70, 130, and 200 m, respectively, and finely divides the mesh near the detonation point, to accurately simulate the propagation process of the explosion shock wave and reduce the workload when the explosion occurs. The detonation depth is uniformly set at 10 m under different water levels in front of the dam, the detonation distance is 10 m, the TNT weight is 1000 kg, and the detonation position is located on the section of the arch crown cantilever, as shown in Figure 22.

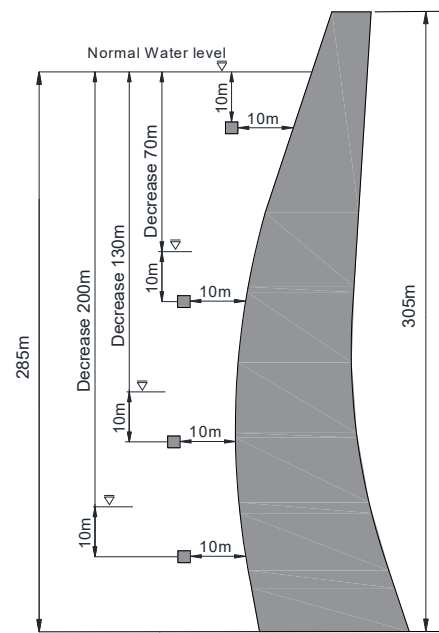


Figure 22. Position of detonation in front of the dam at various water levels.

The analysis of the failure mode and degree of the dam when reducing the water level in front of the reservoir at different amplitudes shows that as the water level in front of the reservoir decreases, so does the damage degree of the dam. When the water level in front of the reservoir falls below the downstream elevation, the dam's anti-explosion performance can be significantly improved, indicating that the water level in front of the dam has a significant impact on the dam's anti-explosion performance.

Due to the water surface cut-off effect, the dam near the free water surface is damaged by cavitation pressure damage when the water level in front of the dam is at its normal water level. Furthermore, the damage level penetrates the dam body and expands with the collapse and tensile damage caused by strong tensile waves on the downstream surface, resulting in penetrating damage and cracking failure of the dam. On the upstream surface of the dam near the initiation center, there is an obvious damage area with a radius of approximately 15 m. There is continuous damage to a depth of approximately 8 m at the dam's crest upstream, and the length of the main damage area accounts for approximately 70% of the length of the arch ring. The damaged area of the dam body's downstream surface is primarily concentrated near the arch crown cantilever at the elevation of the initiation center, and pressure has damaged a portion of the arch dam foundation.

When the water level in front of the dam drops by 70 m, the main damage location on the upstream surface moves closer to the initiation point. There is penetrating damage at the dam abutment on the left bank, and the damage at other locations is less visible. Overall, dam damage is approximately 60% less than when the water level in front of the dam is normal.

The main damage position of the upstream surface drops further when the water level in front of the dam drops by 130 m, and there is a certain degree of damage at the arch ends on both sides of the dam abutment and the foundation surface, but it does not affect the stable operation of the dam body, and the overall damage range of the dam body is smaller than when the normal water level and the water level in front of the dam drop by 70 m.

When the water level in front of the dam drops by 200 m, the upstream surface near the detonation center suffers damage while the downstream surface suffers little. There are some damages with a depth of less than 5 m on both sides of the arch and foundation surface, and the dam body's damage range is much smaller than at a high water level.

The dam body's damage conditions, such as the damage area ratio of the upstream and downstream surfaces, the damage depth of the arch crown cantilever, and the damage

volume ratio of the dam crest under different water levels in front of the dam, are listed, and it can be seen more clearly that the water level in front of the dam affects the dam body’s anti-explosion ability, as shown in Table 6.

Table 6. Failure of the arch dam body due to varying water levels in front of the dam.

The Water Level in Front of the Dam	Damaged Area Ratio (%)		Damaged Depth of Crown Cantilever (m)		Dam Crest Damage Volume Ratio (%)
	Upstream Surface	Downstream Surface	Upstream Surface	Downstream Surface	
Normal water level	12.8	21.2	Penetration		41.1
Water level drops 70 m	10.7	8.5	8.2	0.0	13.6
Water level drops 130 m	8.1	7.8	6.4	0.2	10.5
Water level drops 200 m	7.6	7.5	2.8	0.0	8.3

Table 6 shows that as the water level in front of the dam continues to fall, the damage area ratio between the upstream and downstream surfaces of the dam body decreases, as does the damage volume ratio at the dam crest. It clearly demonstrates that lowering the water level in front of the dam has a significant impact on increasing the anti-explosion capacity of the dam body.

In the case of different water level positions in front of the dam, the damage is averaged along the arch direction of the dam crest and the damage distribution curve is drawn along the arc length of the dam crest, as shown in Figure 23. The dam crest damage curve reflects the main location of damage at the dam crest, with clear interval regional distribution characteristics. The damage at the dam’s top is significantly reduced as the water level in front of the dam drops.

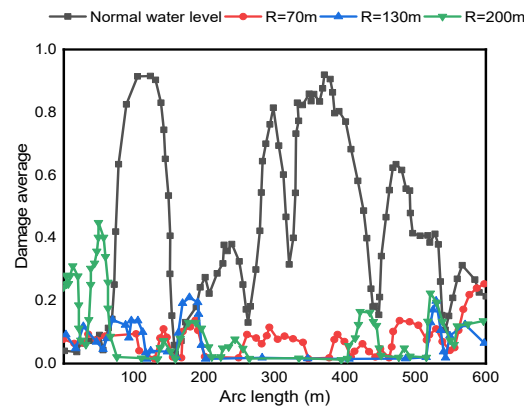


Figure 23. Damage curves for dam crests at various water levels in front of the dam.

The maximum displacement value, maximum velocity value, and maximum acceleration value in the entire dynamic time history of each monitoring point at the arch crown beam are extracted, respectively, to further investigate the dynamic response of the dam body under different water levels in front of the dam, as shown in Figure 24, where R represents the decreased degree of water level.

As shown in Figure 24, the maximum displacement, maximum velocity, and maximum acceleration values of each monitoring point at the arch crown beam position increase near their respective initiation points as the initiation center position changes. This proves that the explosion impact load has the greatest impact on the dynamic response of the monitoring point closest to the detonation center. Furthermore, the monitoring point’s influence on the dynamic response of the monitoring point far away from the detonation center is relatively weak. The greater the distance, the less impactful the influence. By comparing the dynamic responses of each monitoring point at different detonation depths

in Figure 14, it is clear that the decline in water level, rather than the decline in detonation depth, has a strong impact on the weakening of the dam body’s dynamic response.

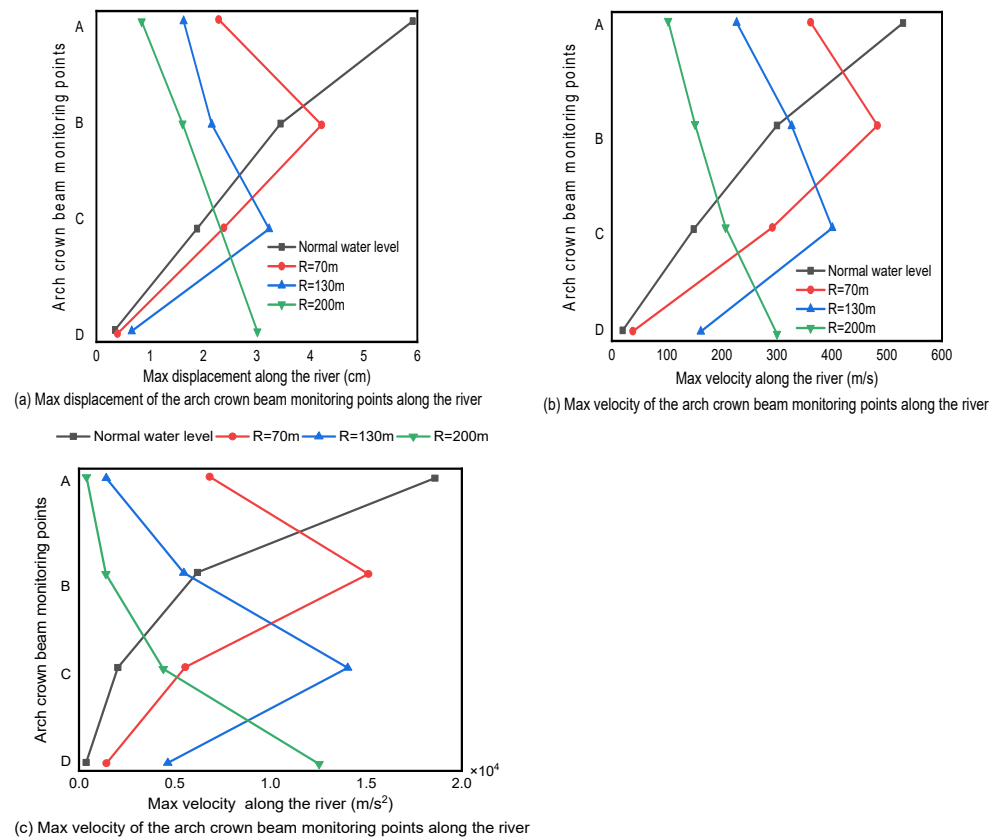


Figure 24. Dynamic response of arch crown cantilever monitoring points in front of the dam at various water levels.

3.5. Prediction of Damage to Concrete Arch Dams Due to An Underwater Explosion Impact Load

3.5.1. Morphological-Based Classification of Concrete Arch Dam Explosion Damage Grade

The response of the structure to explosive loads is a complex physical process that includes explosive detonation, shock wave propagation, blast, and structure dynamic interaction, and the resulting process of structural response, other than static loads and earthquake response, is much more complicated and causes massive damage to the structure. To effectively protect the dam structure’s safety from the action of an explosive impact load, it is necessary to predict the dam’s potential damage and failure state and implement protective measures by the predicted damage and failure state. The current work is difficult to carry out because of the limitations of test conditions and test funds, as well as the insurmountable disadvantages of difficult data acquisition, data error, and environmental impact when the test method is used to predict dam damage and failure under the impact load of an underwater explosion. As a result, the numerical method is used in this section to predict arch dam damage and failure state under the underwater explosion impact load. The most influential factors (the explosive detonation distance and quantity) on the dam damage state are identified based on the damage and failure level proposed in this paper. The typical damage and failure modes and damage characteristics under different failure states are obtained through a large number of working condition calculations, and the dam damage prediction model under an underwater explosion impact is established. Furthermore, the dam damage prediction key curves corresponding to different damage levels are divided, the safe initiation distance of the dam under the impact load of an underwater explosion is obtained, and a damage prediction flow chart is provided, which can serve as a basis and reference for the damage prediction of other dam types.

It is necessary to classify the damage level under an underwater explosion impact load when establishing the damage prediction model under an underwater explosion impact load. This paper divides the failure grades of concrete arch dams under the impact load of the underwater explosion into four categories based on the results of existing literature and the structural characteristics of concrete arch dams:

- (1) No damage: the dam is in the linear elastic working range from its initial state to fewer microcracks.
- (2) Minor damage: from fewer microcracks to crushing and punching failure through one-third of the dam section, the dam will not fail, and the non-linear response and cracking are within acceptable limits.
- (3) Moderate damage: the depth of crushed and broken cracks ranges from one-third to two-thirds of the dam section, and the dam is still repairable.
- (4) Severe damage: The crack depth of crushing and breaking from 2/3 through the dam section to the entire dam section indicates that the dam has been seriously damaged under this failure state, and immediate reconstruction measures are required.

It is worth noting that the classification of damage and failure levels is somewhat subjective. Similar classifications of damage and failure levels can be found in the literature [48,51]. The punching depth is determined by the damage level of the dam. When the dam section's unit damage factor exceeds 0.99, it is assumed that the dam has failed due to cracking.

3.5.2. Understanding the Key Causes of Damage

A fully coupled model of an underwater explosion arch dam under different initiation parameters has been established to identify the most influential factors in the failure state of the dam and determine the safety protection distance of the dam to evaluate the anti-explosion performance of the dam under the impact load of an underwater explosion and predict the damage and failure state of the dam. The damage prediction model of a concrete arch dam under an underwater explosion impact load is established in this section, and changes in dam height and water level in front of the reservoir are not considered temporary. In this paper, numerous working conditions have been calculated, but only some typical results are presented. The computational model's geometric description and boundary conditions are the same as before. The following mesh division principles are used under various calculation conditions: The unit size of the explosive center and the surrounding medium is 100 mm, and the unit size increases proportionally to the detonation center distance; The unit size is 200 mm in the middle and upper parts of the dam, and it is appropriately increased towards the bottom of the dam.

The previous analysis shows that the detonation distance, detonation depth, and amount of explosives all have a significant impact on the dam's failure mode. However, for shallow water explosions, when the initiation depth changes from 10 to 40 m, the dam's failure mode drastically changes, but when the dam damage classification suggested above is used, the dam's damaged state is all serious failure state. As a result, when predicting dam damage and failure state, this paper assumes that the study is conducted at the same initiation depth. The following analysis will use 20 m as the typical initiation depth, and the initiation distance and explosive quantity will be determined as the two main factors influencing the dam's damage level. To investigate the dynamic response and damage and failure state of a dam under the action of an underwater explosion impact load, the initiation distance was varied from 2 to 30 m, and the corresponding explosive amount was varied from 100 to 1000 kg at each initiation distance, to determine the dam damage and failure level corresponding to different initiation distances and different explosive amounts. The analysis reveals some typical minor, moderate, and severe damage to the concrete arch dam induced by an underwater explosion impact load. The given typical failure states of concrete arch dams show that as the explosive volume increases, so does the damage degree of the arch dam, which is reflected in the increasing damage area ratio of the upstream surface to the downstream surface and the damage volume ratio of the dam crest.

Furthermore, the damaged area of the dam body’s downstream surface is significantly larger than that of the dam body’s upstream surface, and the damage to the arch crown cantilever gradually reaches penetration. The dam crest damage reveals the interval area distribution characteristics and presents a symmetrical distribution with the explosion point as the center. The maximum values of displacement, velocity, and acceleration of each monitoring point increase as the explosive equivalent increases. When high-energy explosives are detonated near the upstream dam surface (the initiation distance range is 2~5 m), even if the explosive equivalent is small, serious crushing damage occurs on the upstream surface of the dam facing the explosive center, primarily due to less attenuation of the high-pressure shock wave generated after explosive initiation, which directly acts on the dam surface and will crush the dam surface concrete. At a short initiation distance, blasting pits appear on the dam surface. When the initiation distance gradually increases, the dam damage gradually decreases under the same amount of explosives. The greater the amount of high explosive used at the same initiation distance, the greater the dam damage. The analysis also shows that, as a result of the cut-off effect of the dam’s free water surface, some minor, moderate, or even serious damage occurs near the dam’s free water surface.

3.5.3. Underwater Blast Damage Prediction Model for Concrete Arch Dams

A large number of cumulative damage effects of concrete arch dams under the impact load of underwater explosions are analyzed to obtain the relationship curve between the amount of explosive and the detonation distance. The dam damage grade diagram corresponding to the initiation distance and explosive quantity is obtained through statistical analysis of the calculation results of several working conditions, as shown in Figure 25. The curve fitting method is used to obtain the prediction curve for arch dam damage and failing grade, and two different damage and failure levels are represented on both sides of each curve.

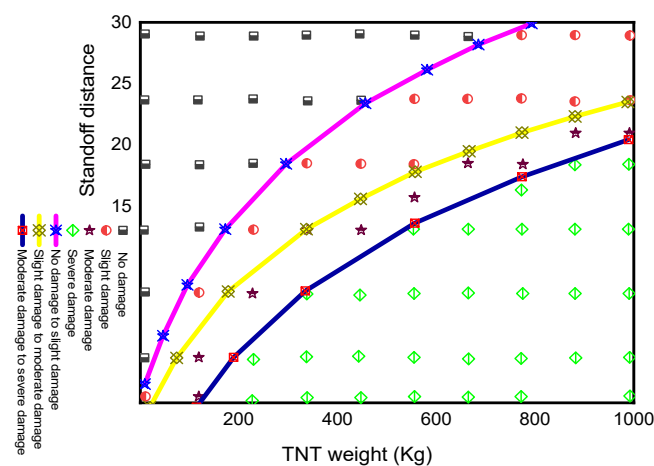


Figure 25. Prediction curve of the degree of dam damage.

The first curve in Figure 25 corresponds to the dam’s critical curve from no damage to minor damage and failure. The coordinate point on the left side of the curve indicates that under the corresponding explosive amount and initiation distance, the dam will not be damaged.

The relationship of the fitting curve can be expressed using the curve fitting method as

$$13.36 \ln(C_w) - 58.67(2 m \leq R \leq 30 m) \tag{39}$$

In the formula, R denotes the detonation distance (m); C_w is the explosive charge weight (kg).

The second curve in Figure 25 corresponds to the dam's critical curve, which ranges from minor to moderate damage. The relationship of the second curve can be expressed using the method of curve fitting based on the numerical calculation results

$$10.71 \ln(C_w) - 49.13 (2 \text{ m} \leq R \leq 30 \text{ m}) \quad (40)$$

The detonation distance and explosive charge are represented by the point between the first and second curves. The dam will sustain minor damage on both the upstream and downstream sides.

The third curve in Figure 25 corresponds to the dam's critical curve, which ranges from moderate to severe damage. The fitted curve's relationship can be expressed as

$$12.31 \ln(C_w) - 63.51 (2 \text{ m} \leq R \leq 30 \text{ m}) \quad (41)$$

The corresponding explosive quantity and initiation distance are indicated by the point between the second and third curves. The dam will sustain moderate damage as a result of its failure. Under the corresponding explosive volume and detonation distance, the point below the third curve indicates that the dam will be severely damaged. It should be noted that, due to the complexity of the numerical calculation model and the calculation time, the damage prediction curve provided does not account for the effect of underwater explosion bubble fluctuating pressure and is only appropriate for predicting the damage and failure state of a concrete arch dam under a shallow water explosion impact load.

According to the dam damage level corresponding to the initiation distance and explosive amount shown in Figure 25, the initiation conditions such as initiation distance and explosive amount have a significant impact on the concrete arch dam's anti-explosion performance. The safe detonation distance under different explosive amounts can be effectively evaluated using the damage prediction curve in the figure. When a 1000 kg TNT explosive is detonated underwater, for example, the safe initiation distance to avoid serious dam damage is at least 21.5 m. When the amount of TNT explosive used is 500 kg, the safe initiation distance is approximately 13 m. Because the research results presented above are for specific concrete arch dams, Figure 26 depicts the flow chart for developing a damage prediction model for a concrete arch dam subjected to an underwater explosion impact load. The corresponding damage prediction curve for a given dam section can be determined using the flow chart. More influencing factors must be considered in future research to more quickly and accurately predict the anti-explosion performance of concrete arch dams under explosion impact loads.

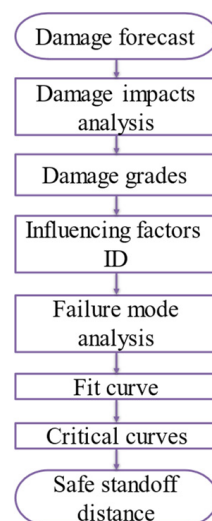


Figure 26. Flow chart for creating a damage prediction model for a concrete arch dam subjected to an underwater explosion impact.

3.6. Anti-Explosion Protection Measures for Arch Dams

The Protective Effect of Aluminum Foam on the Dam Body's Anti-Knock Performance

The method of applying a certain thickness of aluminum foam to the upstream surface of the concrete arch dam is used to study the improvement of the anti-explosion performance of concrete arch dams with aluminum foam. In this section, 0.2 m of thick aluminum foam is added upstream of the entire dam body as a protective layer, and the dam body's dynamic response and damage failure under 10 and 80 m of underwater detonation, respectively, are calculated. The damage failure situation is depicted in Figures 27 and 28 in comparison to the dynamic response and damage failure results of the dam without aluminum foam. The detonation distance is 10 m, the TNT is 1000 kg, and the detonation position is on the crown cantilever section of the arch. As shown in Figures 27 and 28, the damage to the dam body with and without an aluminum foam protective layer shows that aluminum foam has a very good effect on improving the explosion-proof performance of the dam body. When the underwater 10 m explodes with the foam aluminum protective layer, there is minor damage with a radius of 3 m on the upstream surface of the dam body near the initiation point, and the damage on the dam crest, abutment, and foundation surface on both sides is significantly less than without the aluminum foam protective layer. The damage degree will be reduced further when the 80 m underwater explodes with a foamed aluminum protective layer. The damage to the dam body as a whole will not affect the dam body's normal and stable operation. Only minor repairs are required to return the dam body to its original condition. This proves that aluminum foam has a significant protective effect on the arch dam and can significantly reduce the damage caused by explosion load, improve the dam's anti-explosion performance, and effectively protect the dam.

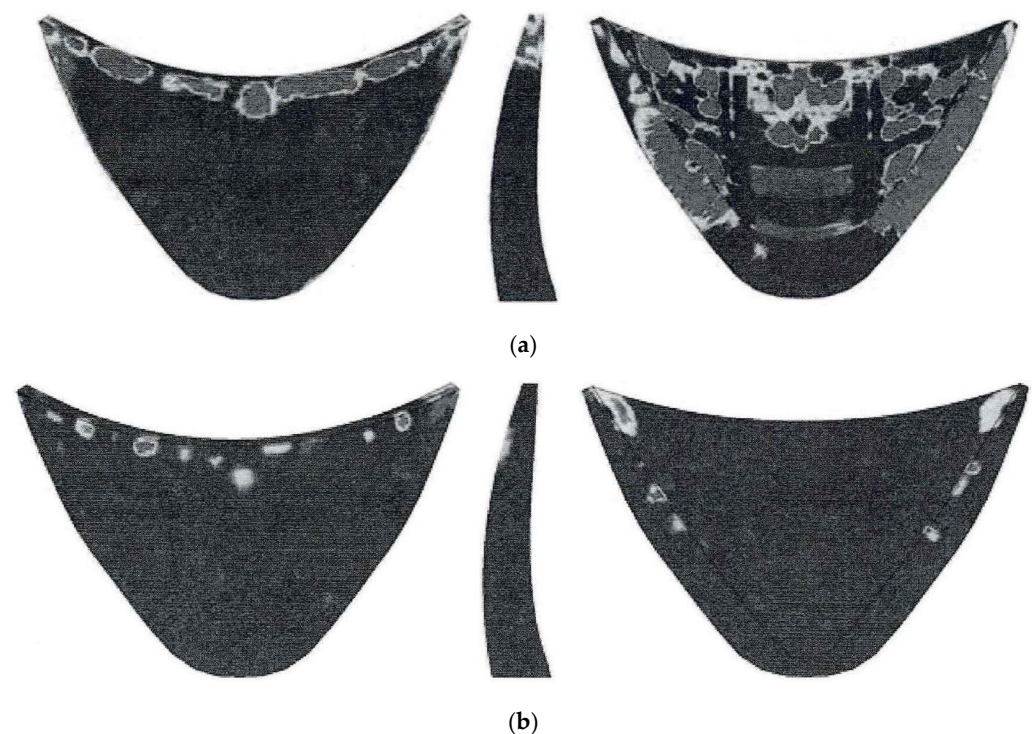


Figure 27. Arch dam damage cloud chart with 10 m underwater initiation. (a) Upstream surface, arch crown cantilever, and downstream surface view damage cloud chart without a foamed aluminum protective layer. (b) Upstream surface, arch crown cantilever, and downstream surface view damage cloud chart with a foamed aluminum protective layer.

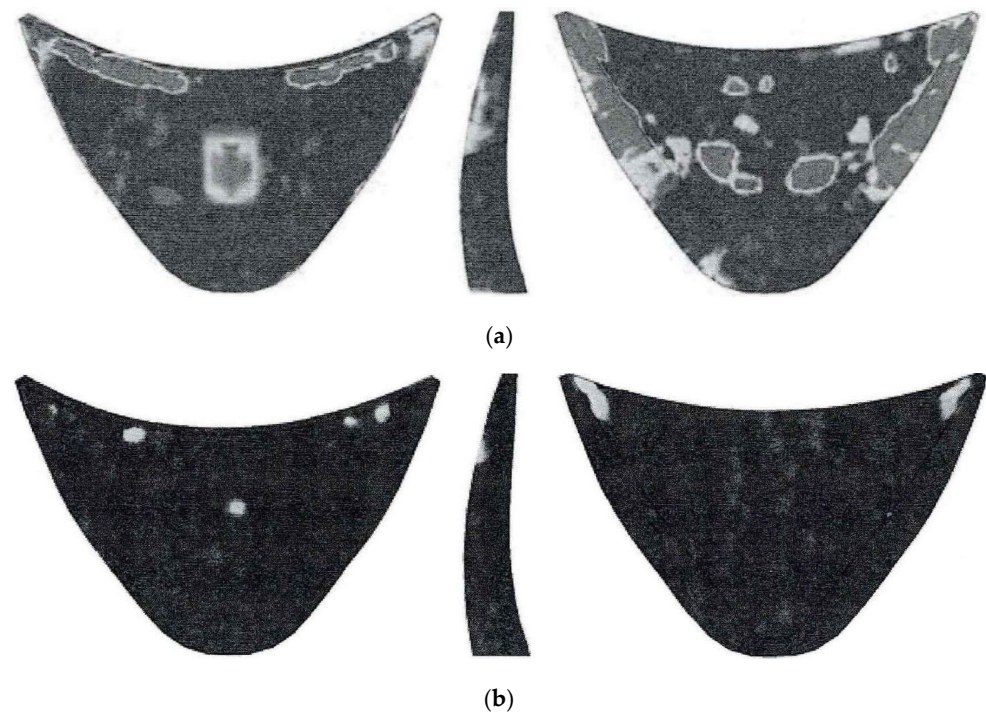


Figure 28. Arch dam damage cloud chart with 80 m underwater initiation. (a) Upstream surface, arch crown cantilever, and downstream surface view damage cloud chart without a foamed aluminum protective layer. (b) Upstream surface, arch crown cantilever, and downstream surface view damage cloud chart with a foamed aluminum protective layer.

Damage to the dam body can be seen more clearly, such as the damaged area ratio of the upstream and downstream surfaces, the damaged depth of the arch crown cantilever, and the damaged volume ratio of the dam crest without and with the foamed aluminum protective layer. Table 7 depicts the protective effect of the foamed aluminum protective layer on the anti-blast of the dam body. Table 7 clearly shows that foamed aluminum has a protective effect on the dam. Applying a protective layer of foamed aluminum can effectively reduce the damage area ratio of the dam’s upstream and downstream surfaces, as well as the damage volume ratio of the dam crest position, which can reduce the damage depth of the arch crown cantilever section, thereby improving the dam body’s anti-explosion ability.

Table 7. Dam body damage with and without the foamed aluminum protective layer.

The Protective Layer Thickness and Surface	Damaged Area Ratio (%)		Damaged Depth of Arch Crown Cantilever (m)		Dam Crest Damaged Volume Ratio (%)
	Upstream Surface	Downstream Surface	Upstream Surface	Downstream Surface	
without foamed aluminum protective layer, H = 10 m	12.8	21.2	Penetration		41.1
with foamed aluminum protective layer, H = 10 m	10.7	2.6	0.4	0.0	5.3
without foamed aluminum protective layer, H = 80 m	11.5	14.4	4.8	0.2	27.6
With the foamed aluminum protective layer, H = 80 m	0.5	0.7	0.2	0.0	1.2

Figures 29 and 30 depict the dynamic response of the dam body to the explosion impact load with and without the aluminum foam protective layer. The former corresponds to the

dynamic response of the dam crest monitoring point, while the latter refers to the dynamic response of the arch crown cantilever monitoring point.

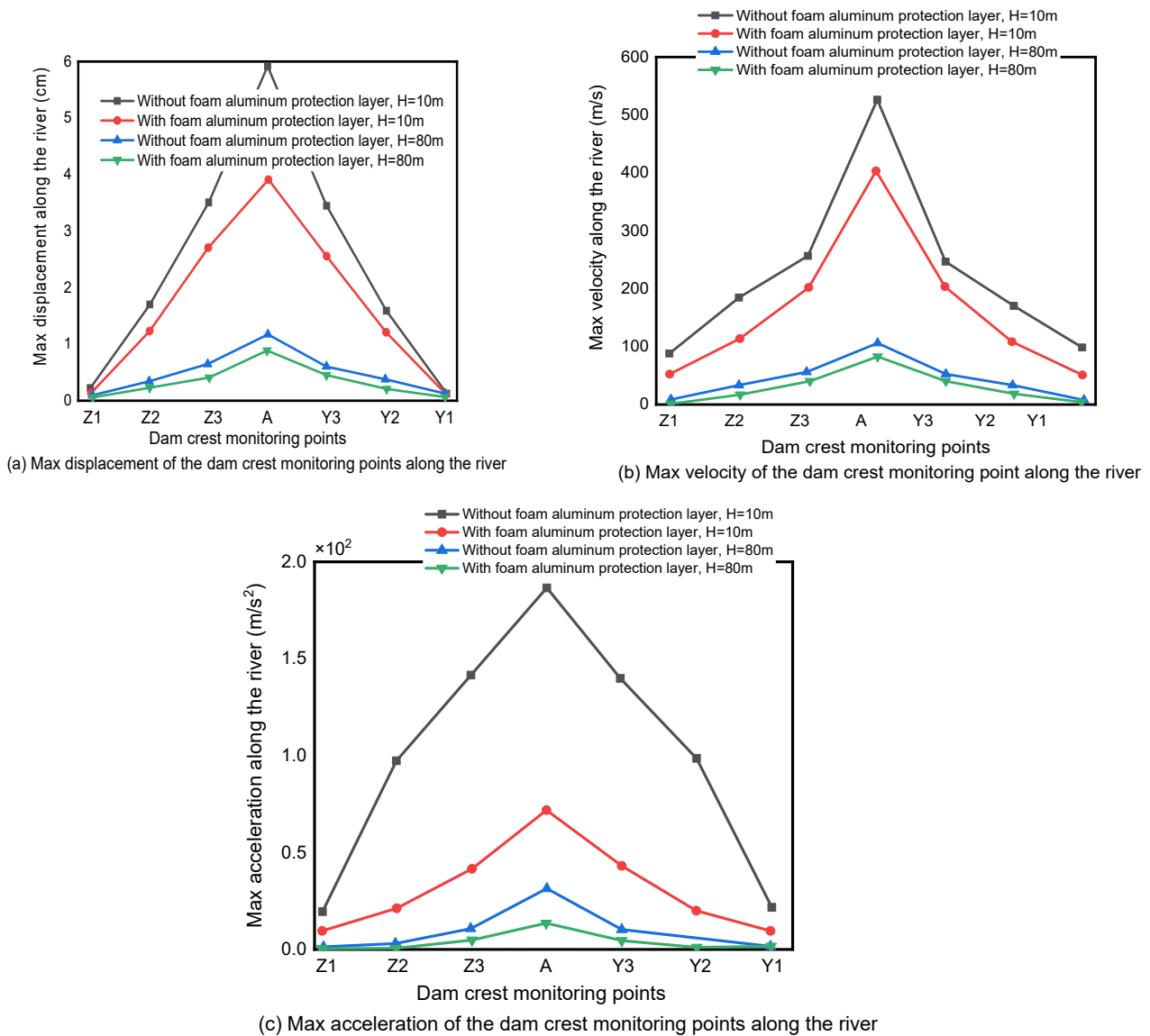
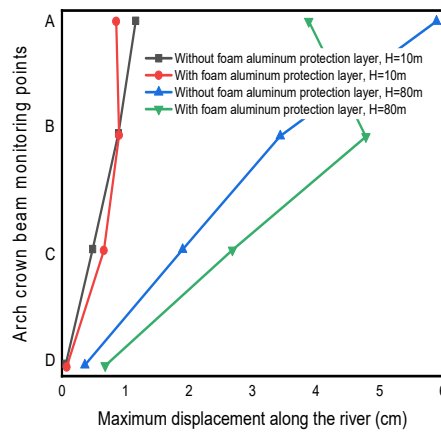
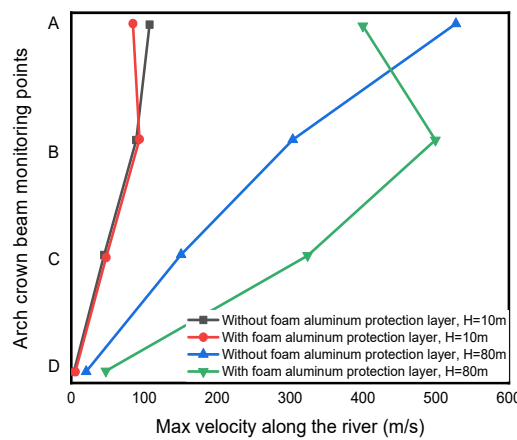


Figure 29. Dynamic response of dam crest monitoring point with and without a foamed aluminum protective layer.

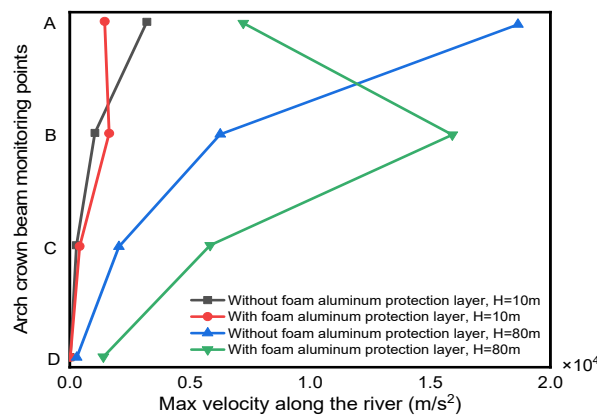
Figures 29 and 30 show that when a foamed aluminum protective layer is existent, regardless of the depth of the underwater detonation, the dynamic response of the dam body can be effectively reduced and the dam body’s stability can be improved. This is because most of the blast waves are absorbed by the foamed aluminum material, and the energy transferred to the dam is not very large, resulting in a relatively low dam response.



(a) Max displacement of arch crown beam monitoring point along the river



(b) Max velocity of arch crown beam monitoring points along the river



(c) Max acceleration of the arch crown beam monitoring points along the river

Figure 30. Dynamic response of an arch crown cantilever monitoring point without and with an aluminum foam protection layer.

4. Conclusions and Suggestions

Dam safety and protection from strong explosions deserve special attention given the obvious seriousness of the consequences. This paper addresses improving the anti-explosion safety of major hydraulic structures by revealing the dynamic response behavior, damage mechanism, and dam characteristics under explosion impact loads, as well as evaluating the dam’s condition after extreme loads. In the critical work of disaster prevention and mitigation, this is crucial to our social and economic development. The following conclusions are drawn from this research:

1. The crack distribution of reinforced concrete slabs under blast impact load obtained by the Lagrangian and Eulerian coupling method is consistent with the distribution law of test results, indicating that the numerical model adopted in this paper can effectively predict the dynamic response and failure process of structures under blast impact load.
2. As the initiation depth increases, so does the overall damaged volume of the arch dam. Near their respective initiation points, the maximum value of displacement, velocity, and acceleration of each monitoring point at the position of the arch crown cantilever is maximized. Dam damage is concentrated primarily on the upstream and downstream surfaces, as well as the dam crest near the detonation center, including the foundation surface on both sides near the arch ends and at the same elevation as the detonation center. The damaged area of the dam's upstream surface is smaller than the damaged area of the dam's downstream surface as a whole. The dam crest damage is symmetrically distributed with the detonation center and has interval area distribution characteristics. The direct impact of the explosion load is primarily responsible for the damage to the upstream surface near the detonation center. The downstream surface near the detonation center suffers direct impact damage from the detonation load as well as tensile damage from the reflection of the blast shock wave. The dam crest damage is caused by tensile damage caused by the reflection of the blast shock wave, as well as cumulative damage caused by the violent dynamic response effect at the dam crest. It is a compression failure when the burst impact load transmits the force to the rock mass on both banks through the arch ring causing damage to the arch end and foundation surface. Furthermore, as the detonation depth increases, so does the thickness of the dam near the detonation center, and the overall damage to the dam is caused by the explosion load, which is affected by the thickness of the dam. The position of the dam crest and arch end are the weak parts of the dam's detonation-proof, according to the above analysis of the dam's damaged area.
3. As the detonation distance increases, the dam body's dynamic behavior and damage failure decrease. As can be seen, a long-distance bang improves the dam body's explosion proofing. As a result, in the event of war, an isolation net can be added in front of the dam to prevent the explosion from occurring near the dam body, thereby protecting the dam body to the greatest extent possible.
4. The position of the detonation center has a significant impact on the dam body's dynamic response and failure. The overall damage to the dam body decreases as the detonation center moves from the crown cantilever position to the arch end on one side, and the local damage keeps moving to the arch end as the detonation center position changes. With the movement of the detonation center, the monitoring point of the dam crest position with the maximum dynamic response also changes. In general, the explosion at the position of the arch crown cantilever is the most detrimental to the dam body's anti-explosion.
5. The damage degree of the arch dam as a whole is decreasing as the water level in front of the dam continues to fall. Near their respective detonation points, the maximum value of displacement, velocity, and acceleration of each monitoring point at the position of the arch crown cantilever is maximized. In comparison to the decline in detonation depth, the results show that the decline in water level has a greater impact on the overall anti-blast capacity of the arch dam body than the decline in detonation depth. As a result, lowering the reservoir level in front of the dam is an effective civil air defense measure for reducing the dynamic response of the dam body, improving the anti-explosion performance of the dam, and reducing the loss of the accident risk during the war. So that as much of the dam body as possible is not submerged in water, and to avoid the massive damage caused by an underwater explosion of high-water level to the dam body.
6. According to the suggested damage level, the dam damage prediction model under an underwater explosion impact is established, and the dam damage prediction curves

corresponding to different damage levels are divided, which can effectively predict the safe initiation distance under different explosive quantities.

7. The addition of foamed aluminum upstream of the dam body can effectively protect the dam body, reduce the dynamic response and damage failure of the dam body, and significantly improve the dam body's anti-explosion ability.

Author Contributions: Conceptualization, S.M.M.; Funding acquisition, G.L. and Z.S.; Methodology, S.M.M. and J.Z.; Project administration, G.L.; Resources, G.L. and Z.S.; Software, J.Z., G.F.E. and V.E.S.; Validation, G.L. and Z.S.; Visualization, G.F.E.; Writing—original draft, S.M.M. All authors have read and agreed to the published version of the manuscript.

Funding: This work was supported by the Natural Science Foundation of Jiangsu Province (520042711) and The Special Project for Free Exploration of Basic Research Funds for the Central Universities (B200203039).

Institutional Review Board Statement: Not applicable.

Informed Consent Statement: Not applicable.

Data Availability Statement: The data used to support the findings of this study are included in this article.

Conflicts of Interest: The authors declare that they have no known competing financial interest or personal relationships that could have appeared to influence the work reported in this paper.

References

1. Zhang, C.; Gholipour, G.; Mousavi, A.A. Blast loads induced responses of RC structural members: State-of-the-art review. *Compos. Part B Eng.* **2020**, *195*, 108066. [CrossRef]
2. Wang, Z.; Hu, K.; Zhao, Y. Doom-roof steel tanks under external explosion: Dynamic responses and anti-explosion measures. *J. Constr. Steel Res.* **2022**, *190*, 107118. [CrossRef]
3. Zhang, H.; Jin, C.; Wang, L.; Pan, L.; Liu, X.; Ji, S. Research on dynamic splitting damage characteristics and constitutive model of basalt fiber reinforced concrete based on acoustic emission. *Constr. Build. Mater.* **2021**, *319*, 126018. [CrossRef]
4. Li, Q.; Zhang, C.; Wang, G. Dynamic damage constitutive model of concrete in uniaxial tension. *Eng. Fract. Mech.* **1996**, *53*, 449–455. [CrossRef]
5. Fu, Q.; Bu, M.; Xu, W.; Chen, L.; Li, D.; He, J.; Kou, H.; Li, H. Comparative analysis of dynamic constitutive response of hybrid fibre-reinforced concrete with different matrix strengths. *Int. J. Impact Eng.* **2020**, *148*, 103763. [CrossRef]
6. Yu, X.; Li, C.; Fang, Q.; Zheng, R.; Jian, H.; Xiang, H. A concrete constitutive model considering coupled effects of high temperature and high strain rate. *Int. J. Impact Eng.* **2017**, *101*, 66–77. [CrossRef]
7. Wu, X.; Wang, S.; Yang, J.; Zhao, J.; Chang, X. Damage characteristics and constitutive model of lightweight shale ceramsite concrete under static-dynamic loading. *Eng. Fract. Mech.* **2021**, *259*, 108137. [CrossRef]
8. Brown, S. Famous Inventors. 2022. Available online: <https://www.famousinventors.org/> (accessed on 10 May 2022).
9. Rodionov, M.; Osborn, A. Russian Troops Destroy Ukrainian Dam That Blocked Water to Crimea-RIA. MOSCOW (Reuters). Available online: <https://www.usnews.com/news/world/articles/2022-02-26/russian-troops-destroy-ukrainian-dam-that-blocked-water-to-crimea-ria> (accessed on 10 May 2022).
10. Ukraine Crisis Media Center. *The Russian Occupiers Tried to Blow up the Dam of the Kyiv Reservoir*; Ukrainian House: Kyiv, Ukraine, 2022; Available online: <https://uacrisis.org/en/the-russian-occupiers-tried-to-blow-up-the-dam-of-the-kyiv-reservoir> (accessed on 10 May 2022).
11. Fan, Q.; Zhou, S.; Yang, N. Optimization design of foundation excavation for Xiluodu super-high arch dam in China. *J. Rock Mech. Geotech. Eng.* **2015**, *7*, 120–135. [CrossRef]
12. Xia, Y.; Li, C.; Zhao, X.; Zhang, Z. Mechanism Research of Arch Dam Abutment Forces during Overload. *Math. Probl. Eng.* **2015**, *2015*, 1–12. [CrossRef]
13. Zhao, X.; Fang, H.; Wang, G.; Fan, Y. Safety Evaluation of Arch Dam Subjected to Underwater Contact Explosion. *Mathematics* **2021**, *9*, 2941. [CrossRef]
14. Pan, X.; Wang, G.; Lu, W.; Yan, P.; Chen, M.; Gao, Z. The effects of initial stresses on nonlinear dynamic response of high arch dams subjected to far-field underwater explosion. *Eng. Struct.* **2022**, *256*, 114040. [CrossRef]
15. Shi, R.; Qu, Y.; Batra, R.C. Numerical simulation of underwater explosion wave propagation in water–solid–air/water system using ghost fluid/solid method. *J. Fluids Struct.* **2019**, *90*, 354–378. [CrossRef]
16. Paydar, S.; Sharifian, M.; Parvaz, S. Explosive attack: Lessons learned in Seyed Al Shohada mosque attack, April 2008, Shiraz, Iran. *J. Emerg. Trauma Shock* **2012**, *5*, 296–298. [CrossRef] [PubMed]
17. Díaz, A.F.; González, F.E.; Francisco, S.P.J. Characteristic overpressure-impulse-distance curves for the detonation of explosives, pyrotechnics or unstable substances. *J. Loss Prev. Process Ind.* **2006**, *19*, 724–728. [CrossRef]

18. Desroches, M.; Kaper, T.; Krupa, M. Mixed-mode bursting oscillations: Dynamics created by a slow passage through spike-adding canard explosion in a square-wave burster. *Chaos* **2013**, *23*, 46106. [CrossRef] [PubMed]
19. Brode, H.L. Numerical Solutions of Spherical Blast Waves. *J. Appl. Phys.* **1955**, *26*, 766–775. [CrossRef]
20. Wang, G.; Zhang, S. Damage prediction of concrete gravity dams subjected to underwater explosion shock loading. *Eng. Fail. Anal.* **2014**, *39*, 72–91. [CrossRef]
21. Huang, X.P.; Hu, J.; Zhang, X.D.; Zhang, Z.T.; Kong, X.Z. Bending failure of a concrete gravity dam subjected to under-water explosion. *J. Zhejiang Univ.-SCIENCE A* **2020**, *21*, 976–991. [CrossRef]
22. Zhuang, T.-S.; Wang, M.-Y.; Wu, J.; Yang, C.-Y.; Zhang, T.; Gao, C. Experimental investigation on dynamic response and damage models of circular RC columns subjected to underwater explosions. *Def. Technol.* **2019**, *16*, 856–875. [CrossRef]
23. Ma, S.; Chen, Y.; Wang, Z.; Wang, J.; Lyu, L.; Wei, W. Similarity Law between Centrifuge Scale Test and Prototype Underwater Explosion. *Shock. Vib.* **2021**, *2021*, 8582026. [CrossRef]
24. Zhang, K.; Lu, F.; Peng, Y.; Li, X. Study on dynamic response of gravity dam under air blast load based on similarity law. *Eng. Fail. Anal.* **2022**, *138*, 106225. [CrossRef]
25. Deng, G.-Q.; Yu, X. Numerical study on the case effect of a bomb air explosion. *Def. Technol.* **2020**, *17*, 1461–1470. [CrossRef]
26. Jia, J.; Zhu, J.; Niu, W.; Zhang, J. Influence of acetylene on methane–air explosion characteristics in a confined chamber. *Sci. Rep.* **2021**, *11*, 13895. [CrossRef]
27. Zhong, B.-L.; Wang, J.; Huang, J.-M. Hui. Study on the similarity law of TNT explosion overpressure in air. *Huozhayao Xuebao/Chin. J. Explos. Propellants* **2010**, *33*, 32–35.
28. PowerChina. The Jinping-I Double Curvature Arch Dam Sets New World Record. Power Construction Corporation of China. 2016. Available online: http://www.chinadaily.com.cn/m/powerchina/2016-12/28/content_27870606.htm (accessed on 10 May 2020).
29. Weathersby, J. Investigation of Bond Slip between Concrete and Steel Reinforcement under Dynamic Loading Conditions. Ph.D. Thesis, The Department of Civil and Environmental Engineering, Mississippi State University, Oktibbeha County, MS, USA, 2003. Available online: <https://www.proquest.com/openview/9dab427bd7cc851edb27d5fe442bb73c/1?pq-origsite=gscholar&cbl=18750&diss=y> (accessed on 10 May 2020).
30. Tu, Z.; Lu, Y. Evaluation of typical concrete material models used in hydrocodes for high dynamic response simulations. *Int. J. Impact Eng.* **2009**, *36*, 132–146. [CrossRef]
31. Malvar, L.; Ross, C. Review of strain rate effects for concrete in tension. *Ac Mater. J.* **1998**, *95*, 735–739.
32. Bischoff, P.H.; Perry, S.H. Compressive behaviour of concrete at high strain rates. *Mater. Struct.* **1991**, *24*, 425–450. [CrossRef]
33. Riedel, W. Beton unter Dynamischen Lasten: Meso-und Makromechanische Modelle und ihre Parameter. Ph.D. Thesis, EMI-Bericht, London, UK, 2000.
34. Riedel, W.; Thoma, K.; Hiermaier, S. Penetration of reinforced concrete by BETA-B-500 numerical analysis using a new macroscopic concrete model for hydrocodes. In Proceedings of the 9th International Symposium on the Effects of Munitions with Structures, Berlin, Germany, 3–7 May 1999.
35. Johnson, G.; Holmquist, T. A Computational Constitutive Model for Brittle Materials Subjected to Large Strains, High Strain Rates, and High Pressure. In Proceedings of the EXPLOMET Conference, San Diego, CA, USA, 12–17 August 1990.
36. Johnson, G.; Cook, W. Fracture characteristics of three metals subjected to various strains, strain rates, temperatures and pressures. *Eng. Fract. Mech.* **1985**, *21*, 31–48. [CrossRef]
37. Johnson, G.R.; Holmquist, T.J. An improved computational constitutive model for brittle materials. *AIP Conf. Proc.* **1994**, *309*, 981–984. [CrossRef]
38. Wang, W.; Zhang, D.; Lu, F.; Wang, S.-C.; Tang, F. Experimental study on scaling the explosion resistance of a one-way square reinforced concrete slab under a close-in blast loading. *Int. J. Impact Eng.* **2012**, *49*, 158–164. [CrossRef]
39. Exxentis-Porous-Aluminum. Aluminum Foam-Overview-Types-Production-Applications. Exxentis. 2021. Available online: <https://www.exxentis.co.uk/porous-aluminum/porous-aluminum-technology/aluminium-foam-overview-types-production-applications/> (accessed on 10 May 2022).
40. Xu, Z.; Chen, Z.; Yang, S. Effect of a new type of high-strength lightweight foamed concrete on seismic performance of cold-formed steel shear walls. *Constr. Build. Mater.* **2018**, *181*, 287–300. [CrossRef]
41. Nuri, Y.; Donghoon, S.; Changsu, S.; Sung-Woong, J. Experiments on Blast Protective Systems using Aluminum Foam Panels. *KSCE J. Civ. Eng.* **2014**, *18*, 2153–2161.
42. Sritam, S.S.; Siva, R.G.I.; Selija, K. State-of-the-Art Review on the Characteristics of Surfactants and Foam from Foam Concrete Perspective. *J. Inst. Eng. (India) Ser. A* **2018**, *99*, 391–405. [CrossRef]
43. Chen, G.; Zhang, P.; Liu, J.; Cheng, Y.; Wang, H. Experimental and numerical analyses on the dynamic response of aluminum foam core sandwich panels subjected to localized air blast loading. *Mar. Struct.* **2019**, *65*, 343–361. [CrossRef]
44. Yao, S.; Chen, Z.; Xu, P.; Li, Z.; Zhao, Z. Experimental and Numerical Study on the Energy Absorption of Polyurethane Foam-Filled Metal/Composite Hybrid Structures. *Metals* **2021**, *11*, 118. [CrossRef]
45. Paul, A.; Ramamurty, U. Strain rate sensitivity of a closed-cell aluminium foam. *Mater. Sci. Eng.* **2000**, *281*, 1–7. [CrossRef]
46. Deshpande, V.; Fleck, N. High strain rate compressive behavior of aluminium alloy foam. *Int. J. Impact Eng.* **2000**, *24*, 277–298. [CrossRef]
47. Luccioni, B.; Ambrosini, D.; Danesi, R. Blast load assessment using hydrocodes. *Eng. Struct.* **2006**, *28*, 1736–1744. [CrossRef]

48. Zhou, X.Q.; Hao, H. Numerical Prediction of Reinforced Concrete Exterior Wall Response to Blast Loading. *Adv. Struct. Eng.* **2008**, *11*, 355–367. [[CrossRef](#)]
49. Cole, R. *Underwater Explosions*; Princeton Univ. Press: New York, NY, USA, 1948.
50. Kinney, G.F.; Graham, K.J. *Explosive Shocks in Air*; Springer: New York, NY, USA, 1985.
51. Xu, K.; Yong, L. Numerical simulation study of spallation in reinforced concrete plates subjected to blast loading. *Comput. Struct.* **2006**, *84*, 431–438. [[CrossRef](#)]